# Interferon beta signaling and microglial activation in a murine model for age-related macular degeneration


Inaugural-Dissertation

zur
Erlangung des Doktorgrades
der Mathematisch-Naturwissenschaftlichen Fakultät
der Universität zu Köln

vorgelegt von

Anika Lückoff
aus Gießen

Köln 2016

Die vorliegende Dissertation wurde in der Zeit von Juni 2012 bis Mai 2016 in der Arbeitsgruppe Experimentelle Immunologie des Auges an der Augenklinik der Univeristätsklinik Köln unter der Anleitung von Prof. Dr. Thomas Langmann durchgeführt.

Berichterstatter:

| | |
|---|---|
| Erste Prüferin: | Prof. Dr. Elena Rugarli |
| Zweiter Prüfer: | Prof. Dr. Thomas Langmann |

Tag der mündlichen Prüfung: 29. Juni 2016

*Les Ricochets*

Am Ende gibt es einen Stein, der jault
Wenn er beim Spiel über das Wasser springt
Das Wasser zieht bei jedem Aufprall Kreise
Als ob es ruhig rauchend Ringe bliese

Am Ende dieser abgeschliffne Stein, der jault
Wenn er vier-, fünfmal aufzuckt, untergeht
Die Ringe schwappen langsam an das Ufer
Das sich mit kleinen Wellen die trockenen Lippen leckt

Und schwebend sinkt der flache Stein zum Grunde
Er jault nicht mehr und wühlt nur wenig auf
Er legt sich in den Schlamm und liegt sehr lange
Derweil das Wasser oben sich neu bedeckt mit Glätte

Dietrich Lückoff (1957 - 2014)

# Contents

# Summary

Age-related macular degeneration (AMD) is a disease of the retina and the leading cause of vision loss among the elderly in industrial countries. It is characterized by progressive impairment of the visual perception and can be categorized into two distinct forms; wet and dry AMD. Typical hallmarks of wet AMD are chronic activation of the innate immune system in the retina and the ingrowth of blood vessels from the choroid into the retina termed as choroidal neovascularization (CNV). Microglia, the immune competent cells of the retina, play a major role in the induction and advancement of chronic inflammation and CNV development observed during AMD pathogenesis regulating the immune answer and tissue homeostasis. Therefore, strategies to dampen microgliosis present attractive therapeutic options in the treatment of AMD and other retinal degenerative disorders.

Interferon beta (IFN-$\beta$), an endogenous cytokine and signaling molecule, is responsible for essential regulatory functions of the innate immune system and is well known for its anti-angiogenic and immunomodulatory properties. Consequently, IFN-$\beta$ is used as first line treatment of multiple sclerosis, a neuroinflammatory autoimmune disease of the brain.

However, it was previously unknown whether the protective effect is transferable to the retina. Hence, to fill this gap the current study endeavored to determine the effects of IFN-$\beta$ signaling on microglial activation and choroidal neovascularization using a reproducible murine laser-coagulation model of wet AMD.

The results presented in this study reveal a crucial role of IFN-$\beta$ signaling in regulating microglial reactivity and pathological angiogenesis. Global as well as microglia specific interferon-$\alpha$/-$\beta$ receptor (IFNAR) deletion fortified disease severity and progression as evidenced by enhanced microglia reactivity, vessel leakage and CNV development. In contrast, IFN-$\beta$ therapy resulted in a significant reduction of the clinical features associated with the murine laser-coagulation model of wet AMD.

In conclusion, this work indicates a protective role of IFNAR signaling in retinal immune mechanisms and identifies IFN-$\beta$ as a promising new strategy for future therapy approaches to modulate chronic inflammation in retinal degenerative diseases.

# Zusammenfassung

Die altersabhängige Makuladegeneration (AMD) ist eine Erkrankung der Netzhaut, die zu einer progressiven Beeinträchtigung des visuellen Wahrnehmungsvermögens führt. In Industrieländern sind fast 70% der Erblindungen auf AMD zurückzuführen, wobei zwischen der feuchten und trockenen Form unterschieden wird. Zwei typische Merkmale der feuchten AMD sind zum einen das Einwachsen von choroidalen Blutgefäßen in die Netzhaut, auch Neovaskularisierung genannt, und zum anderen die Aktivierung des Immunsystems in Form einer Mikrogliose. Mikrogliazellen, die immunkompetenten Zellen der Netzhaut, sind in beiden Prozessen maßgeblich beteiligt, indem sie die Immunantwort und die Homöostase im Gewebe regulieren. Eine potentielle Behandlungsmöglichkeit der AMD ist das Eindämmen der Mikrogliose mit einer immunmodulatorischen Substanz. Auf diese Weise sollen die neuroprotektiven Eigenschaften der Mikrogliazellen wieder hergestellt werden, um so der Netzhautdegeneration entgegen zu wirken.
Interferon beta (IFN-$\beta$) ist ein körpereigenes Zytokin und Signalmolekül das für grundlegende Funktionen im angeborenen Immunsystem verantwortlich ist und dessen anti-angiogene, als auch immunmodulierende Wirkung bekannt ist. Aufgrund letzterer Eigenschaft findet IFN-$\beta$ zum Beispiel Einsatz bei der Behandlung von Multiple Sklerose, eine neurodegenerative Autoimmunerkrankung des Gehirns. Bisher unbekannt ist, ob sich diese therapeutischen Eigenschaften von IFN-$\beta$ auch auf die Netzhaut übertragen lassen. Das Ziel dieser Arbeit war es daher, den Effekt von IFN-$\beta$ auf die Mikrogliaaktivierung und Angiogenese *in vivo* zu analysieren.
Mithilfe des murinen Laserkoagulation-Modells für feuchte AMD konnte in dieser Arbeit gezeigt werden, dass der Interferon-$\alpha$/-$\beta$ Rezeptor (IFNAR) erheblichen Einfluss auf die Gefäßneubildung und Mikrogliaaktivierung hat. So entwickeln Mäuse, die kein IFNAR exprimieren bzw. deren IFNAR auf Mikrogliazellen ausgeschaltet wurde, eine deutlich verstärkte Mikrogliose und choroidale Neovaskularisierung. Im Gegensatz dazu konnten, im gleichen Modell, größere Schäden der Netzhaut durch die systemische Behandlung von Mäusen mit IFN-$\beta$ verhindert werden. Nach einer 14-tägigen IFN-$\beta$ Therapie sind beide Krankheitssymptome signifikant zurückgegangen.
Zusammenfassend lassen die Ergebnisse dieser Arbeit den Schluss zu, dass der IFNAR-Signalweg eine protektive Wirkung auf die Netzhaut hat. Besonders im Hinblick auf neue Therapieansätze ist IFN-$\beta$ damit eine vielversprechende Substanz, die Anwendung in der Therapie degenerativer Netzhauterkrankungen finden könnte.

# 1 Introduction

## 1.1 The mammalian retina

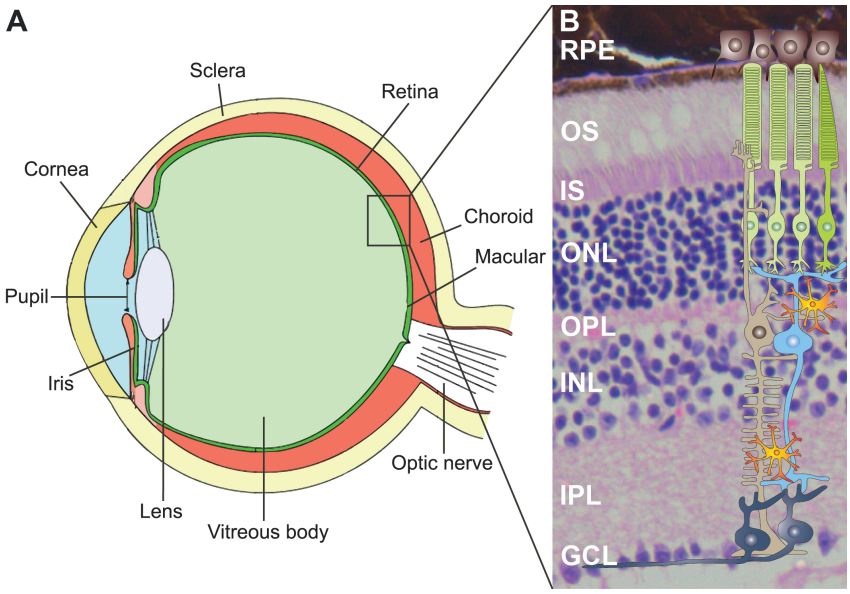


**Figure 1.1:** Anatomy of the mammalian eye and structure of the retina. The retina is the light-sensitive neuronal layer coating the posterior part of the eye. H&E staining of retinal cross section demonstrating distinct structures with schematic overview of different retinal cell types. **Layers** - RPE: retinal pigment epithelium, OS: outer segments, IS: inner segments, ONL: outer nuclear layer, OPL: outer plexiform layer, INL: inner nuclear layer, IPL: inner plexiform layer and GCL: ganglion cell layer. **Cells** - black: retinal pigment epithelial cells, green: rod and cone photoreceptor cells, blue: bipolar cell, grey: ganglion cells, brown: Müller glia cell, orange: microglia cells. (Eye ball modified from: https://upload.wikimedia.org/wikipedia/commons/thumb/a/a5/Eye_scheme.svg/220px-Eye_scheme.svg.png, retinal cross section modified from http://experimentica.com/wp-content/uploads/2013/12/Mouse-retina.-HE.jpg, schematic retinal cells modified from Karlstetter et al. (2010).)

The retina is an approximately 0.2 mm thick neuronal tissue at the posterior part of the eye (Fig. 1.1 A). Compared to the rest of the eye, the retina and the optic nerve evolve during embryonic development from outgrowths of the mesencephalon so that both structures belong next to the brain and the spinal cord to the central nervous system (CNS). When light passes through the cornea and lens, the light-sensitive tissue initiates nerve impulses, which are forwarded by the optic nerve to the visual centers of the brain (Sung and Chuang, 2010).

The retina is organized in several anatomically distinct layers (Fig. 1.1 B). The outer part of the retina, the photoreceptor layer, contains two types of photoreceptor cells, rods and cones, which are both directly light sensitive. Rods support mainly scotopic vision as they function under low light conditions, whereas cones provide photopic vision including a high visual acuity with color perception. The photoreceptors,

which are subdivided in outer (OS) and inner segments (IS), are connected in the outer plexiform layer (OPL) with the bipolar cells, which make synapses with the ganglion cells in the inner plexiform layer (IPL). The optic nerve fibers are formed by the axons of the ganglion cells and process the visual information towards the midbrain and thalamus, where it becomes converted into a picture. Next to the vertical signal transduction, there are laterally arranged horizontal and amacrine cells, providing side-to-side connection. The cell bodies of the above described cell types are either collected in the inner nuclear layer (INL), the outer nuclear layer (ONL) or the ganglien cell layer (GCL) (Nicholls et al., 2001, From Neuron to Brain).
The retinal pigment epithelial (RPE) cells form a monolayer which encloses the photoreceptor outer segments at the apical side and absorbs scattered or unabsorbed light. Additionally, the RPE is known for several other crucial functions including epithelial transport of ions and metabolic end products, phagocytosis of photoreceptor debris and secretion of immunosuppressive factors (Strauss, 2005). Beyond that is the RPE involved in the formation of the blood retina barrier (BRB), a physiological border separating the inner retinal tissue from the blood stream and thereby establishing an immune privileged area.
Apart from that, two more cell types are part of the retina but do not directly contribute to the neuronal signal processing. Müller glia cells span across the whole retina, supporting the neuronal survival and maintaining the homeostasis in the retinal extracellular microenvironment (Bringmann et al., 2006). In contrast, microglia cells are located in the plexiform layers of a healthy retina and monitor their microenvironment as they are the immune competent cells of the tissue (Sung and Chuang, 2010) (see section 1.2 for further information).

### 1.1.1 Degenerative diseases of the retina

The retina is a complex tissue composed of several specialized components, all with a certain susceptibility to genetic defects. For that reason retinal dystrophies are a heterogeneous group of disorders where inherited gene alterations lead to disorganization of the retinal structure causing a defective signal transduction and visual impairment (Sundaram et al., 2012). Until now, the retinal information network (RetNet) database lists 314 identified genes or gene loci with mutations related to retinal dystrophies (https://sph.uth.edu/retnet/disease.htm, May 7$^{th}$ 2016).
On the one hand, there are monogenic diseases like Retinitis Pigmentosa (RP), caused by a wide variety of gene mutations which finally lead to the apoptosis of

photoreceptors (Portera-Cailliau et al., 1994). On the other hand, multifactorial dystrophies become more important as they are the leading cause of visual impairment in industrialized countries. For instance, age-related macular degeneration (AMD) is a complex disease caused by genetic and environmental risk factors as well as aging processes (Jager et al., 2008).
In the past years, various animal models have been developed facilitating research to understand the pathology of degenerative processes but also to develop new therapeutic approaches. There are two fundamentally different types of *in vivo* models: Hereditary models develop retinal tissue degeneration due to genetic manipulation such as the retinoschisin-deficient $Rs1h^{-/Y}$ (Weber et al., 2002) or the $Fam161^{GT/GT}$ mouse (Karlstetter et al., 2014). In $Rs1h^{-/Y}$ mice, retinoschisin knock out leads to a splitting of the inner retinal layers followed by photoreceptor loss. In $Fam161^{GT/GT}$ mice, the truncated Fam161a protein initiates shortened connecting photoreceptor cilia leading to progressive thinning and degeneration of the retina. Secondly, inducible models are used to recapitulate morphological and functional changes of retinal diseases. For example, the laser-coagulation model uses laser injury to disrupt Bruch's membrane leading to choroidal neovascularization (CNV) and strong inflammation of the tissue (Pennesi et al., 2012). Since this model is suitable for animals at different age, genetic background or therapy applications, it is possible to test a broad variety of AMD-influencing factors (Lambert et al., 2013).

### 1.1.2 Age-related macular degeneration

Age-related macular degeneration is a multifactorial degenerative disease of the retina leading to progressive vision impairment up to blindness in the final stage. In 2013, AMD was next to cataracts and glaucoma the most common reason of vision loss (Global burden of disease study, 2015). Due to a continuously aging society, it is expectable that the prevalence of AMD increases in the coming decades.
The disease is subdivided into early and advanced stages. Early age-related macular degeneration is characterized by pigmentation changes and the formation of drusen, an accumulation of intra- and extracellular metabolic debris in the subretinal space of the central retina (Fig. 1.2 A). Later stages of the disease can be classified into either dry AMD with retinal atrophy in the macula or wet AMD with choroidal neovascularization. Although only 10 to 15% of patients suffer from the wet form of AMD, it causes more than 80% of severe visual impairment (Jager et al., 2008). In severe stages of wet AMD, a dysfunctional RPE can cause the detachment of the retina, also called retinal atrophy, which is often accompanied by the expression of

vascular endothelial growth factor (VEGF) and an increased vascular permeability occurring as subretinal hemorrhage or edema exudation (Fig. 1.2 B). Since the release of VEGF stimulates the development of neovessels, choroidal neovascularization proliferates and expands through a porous Bruchs's membrane into the retinal tissue (Fig. 1.2 C) (reviewed in de Jong, 2006).The pathological changes of the retina additionally comes along with a chronic inflammation, which mediates the activation and recruitment of microglia cells from the plexiform layers towards the affected tissue (Karlstetter and Langmann, 2014).

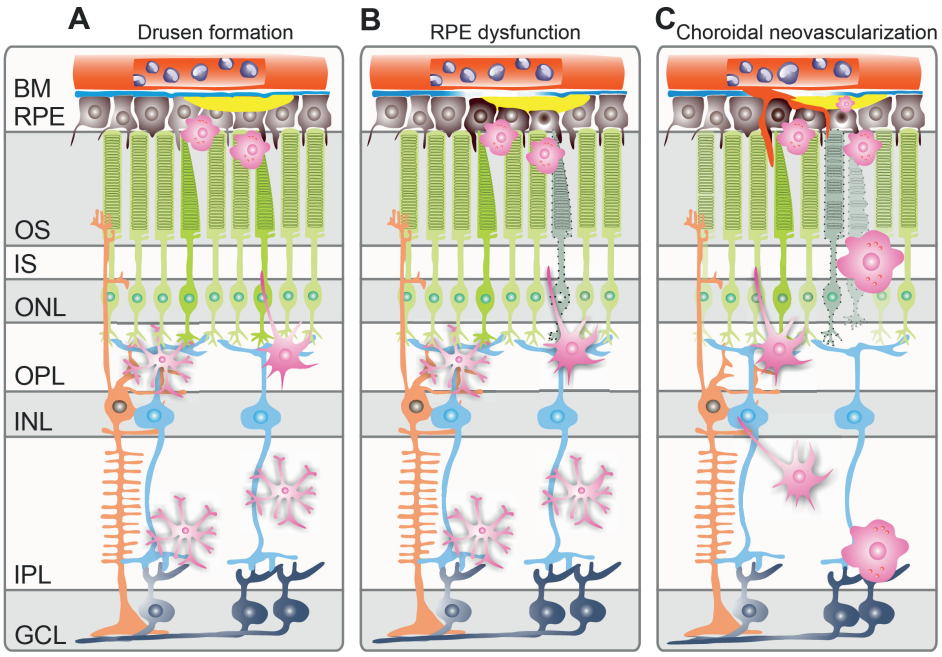


**Figure 1.2:** Schematic development of wet AMD. In early stages of age-related macular degeneration drusen accumulate in the subretinal space. Microglia cells become activated, leave the plexiform layers and migrate towards the outer retina. The dysfunctional RPE promotes in severe stages the ingrowth of choroidal blood vessels into the retina. **Layers** - BM: Bruch's membrane, RPE: retinal pigment epithelium, OS: outer segments, IS: inner segments, ONL: outer nuclear layer, OPL: outer plexiform layer, INL: inner nuclear layer, IPL: inner plexiform layer, GCL: ganglion cell layer. (Scheme modified from Karlstetter et al., 2010).

The major risk factor for disease onset is increasing age. Therefore AMD most commonly occurs in people older than 50 years. But also secondary factors like nutrition, smoking, hypertension, obesity or genetic predisposition influence the development of AMD. Genomic techniques identified mutations in complement factor H (CFH), complement factor B (CFB) and factor C3 as well as age-related

maculopathy susceptibility 2 (ARMS2) genes as risk factors known to predispose their carrier to AMD (Jager et al., 2008).
However, there is currently no effective cure for AMD, but the treatment of isolated clinical symptoms like managing the expansion of CNV can partially restore vision in patients with wet AMD. The most common therapy to attenuate the neovessel sprouting are intravitreal antibody injections inhibiting the vascular endothelial growth factor (VEGF) (Jager et al., 2008). Therefore, potential new therapy options for the management of both, atrophic and neovascular AMD, are of great interest.

## 1.2 Microglia cells

Microglia belong among others to the glia cells and are located in the central nervous system (CNS) consisting of the brain, the spinal cord and the retina. Like macrophages, microglia are mononuclear phagocytes and form the active immune defense in the CNS. They recognize small potentially pathogenic insults and maintain the tissue homeostasis by their phagocytic activity. As resident macrophages of the CNS, they are associated with the pathogenesis of neurodegenerative and inflammatory diseases of the brain and retina (Ginhoux et al., 2010). Approximately 10% of all cells found in the retina are microglia cells, which are typically distributed all over the tissue in large non-overlapping regions, monitoring their microenvironment (Ransohoff and Cardona, 2010).

### 1.2.1 Origin of microglia

Microglia were first described by del Rio-Hortega as cellular element of the CNS using silver staining methods. Back then, he already predicted that microglia enter the brain during early development and that they are of mesodermal origin (del Rio Hortega, 1932).
By now, it is generally accepted that microglia are distinct tissue-specific mononuclear phagocytic cells. They origin from myeloid precursors and represent a distinct cellular entity, different from other cells in the CNS such as neurons, macroglia or vascular cells (Kettenmann et al., 2011; Karlstetter et al., 2015). In contrast to cerebral cells that arise from the primitive neuroepithelium, microglia invade from the yolk sac into the CNS during very early embryonic development before the blood-brain (BBB) and blood-retina barrier (BRB) arise (Ginhoux et al., 2010; Schulz et al., 2012). Both, BBB and BRB are physiological borders formed by endothelial cells,

which separate the CNS from the peripheral tissue and tightly control the intracellular cross-talk and exchange between both compartments (Engelhardt and Liebner, 2014). Because BBB and BRB prevent an unlimited exchange of blood-derived peripheral leukocytes protecting the CNS from a potentially harmful immune response (Streit, 2002), the barrier function is essential for maintaining tissue homeostasis (Liebner et al., 2011). From this the question arises whether microglia cells are a stable, self-maintaining cell population or rather replaced by blood-derived myeloid precursors passing the BBB/BRB for cell renewal. For clarification, parabiosis experiments, in which chimeric mice with differently labeled bone marrow cells share one blood flow, have been performed (Ajami et al., 2007). The results revealed that bone marrow-derived progenitor cells from the periphery do not enter the CNS under both, homeostatic as well as diseased conditions, indicating a slow microglial turnover rate (Gehrmann et al., 1995).
Meanwhile it is widely accepted that microglia are a self-sustaining cell population with a remarkable longevity, which discriminates these cells from peripheral bone-marrow derived cells (Goldmann et al., 2013).

### 1.2.2 Function of microglia

Microglia have different physiological functions within the adult CNS primarily related to immune response as well as maintaining tissue homeostasis. In order to prevent potentially fatal tissue damage, microglia are equally distributed in the plexiform layers of the retina, monitor their microenvironment and react to smallest alterations (see Fig. 1.1 B) (Karlstetter et al., 2010).
Since microglia are the first cerebral immune effector cells, they phagocyte cellular debris and apoptotic cell material, release pro- and anti-inflammatory factors for extracellular signaling and act as important antigen presenting cell in the CNS (Nimmerjahn et al., 2005; van Rossum and Hanisch, 2004; Gehrmann et al., 1995). Once involved in CNS injury, cytotoxic substances like nitric oxigen (NO) and reactive oxygen species (ROS) are released to fight infectious triggers (Banati et al., 1993; Langmann, 2007).
To control microglial neurotoxicity, regulatory ligands like CD200 and C-X3-C motif chemokine ligand 1 (CX3CL1, also named fractalkine) are expressed by neurons and provide, when linked to their respective receptors, calming signals maintaining a homeostatic tissue (Cardona et al., 2006; Combadiere et al., 2007). Both receptors, CD200R and CX3CR1, are highly expressed on microglia cells and have the ability to modulate microglial activity and migration (Carter and Dick, 2004; Kettenmann

et al., 2011). Furthermore, microglia are involved in healing processes as they secrete anti-inflammatory mediators and promote synaptic stripping as well as neuronal regrowth (Gehrmann et al., 1995).

### 1.2.3 Microglia activation

Microglia are highly dynamic cells which are not only characterized by their diverse responsibilities but also by their morphological plasticity. They undergo structural changes and adapt different phenotypes according to their activation status (Gehrmann et al., 1995; Nimmerjahn et al., 2005). In respond to local conditions or detected damage/danger-associated molecular patterns (DAMPs) (Kettenmann et al., 2011; Gao et al., 2011), microglial activation occurs in a graded process (Kreutzberg, 1996). Ramified cells with its small somata and long branching processes transform into activated, round shaped cells, also referred as reactive microglia (Fig. 1.3 from left to right). Once activated, the local density of microglia gain by proliferation to protect and restore tissue homeostasis and the phagocytic activity of the cells increases (Kettenmann et al., 2011). In the retina, reactivate microglia leave the plexiform layers and migrate towards site of damage (Gupta et al., 2003).
Apart from that, activated microglia cells also upregulate the expression of various cell surface molecules such as, major histocompatibility complex proteins II (MHC class II), cluster of differentiation molecule 11b (CD11b, also named integrin alpha-M beta-2 ($\alpha_M\beta_2$)) or ionized calcium binding adaptor molecule 1 (Iba1, also named allograft inflammatory factor 1(AIF1)) (Dick et al., 1995; Xu et al., 2007; Ito et al., 1998; Autieri, 1996), which are amongst others used to immunohistochemistrally distinguish microglia cells from other cerebral/retinal cells. Especially the classical microglial marker protein Iba1 is used to image their morphology in detail (Kettenmann et al., 2011).

### 1.2.4 Microglia in AMD

In human AMD it has been reported that a large amount of activated microglia cells are detectable in the subretinal space as well as the outer nuclear layer. A closer view displayed numerous engulfed photoreceptor particles in these microglia cells (Gupta et al., 2003). During earlier phases of AMD, enlarged phagocytes, either microglia

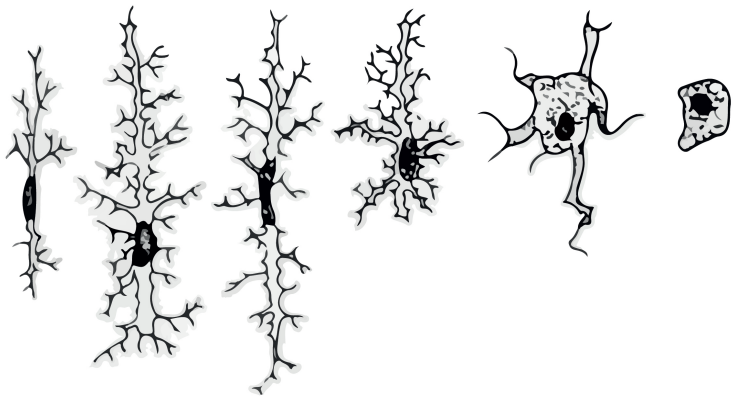

**Figure 1.3:** Different microglia morphology. From left to right: Ramified microglia cells form long branched protrusions around a small cell soma to monitor their microenvironment. Alterations in the tissue homeostasis cause graded morphological changes towards a amoeboid shape, characterized by a rounded cell with an enlarged cell body. (Scheme modified from Kreutzberg, 1996).

or invading macrophages, are also related to subretinal drusen, indicating that they are attracted by the accumulation of lipids and deposits (Killingsworth et al., 1990; Penfold et al., 1985).

Furthermore, transcriptome analysis of donor retinas of previously characterized AMD patients revealed an over-expression of wound response, complement, and gliogenesis genes. Especially the up-regulation of complement and major histocompatibility complex I genes like human leukocyte antigen (HLA)-A/B/C or beta-2 microglobulin (B2M) indicates an activation and contribution of microglia/ macrophages during AMD (Newman et al., 2012).

In murine AMD-models, the induction of retinal damage triggers a quick recruitment and accumulation of monocytes and microglia towards the site of damage before first indications of CNV are visible (Eter et al., 2008; Ebert et al., 2012). Interestingly, depleting these cells with a monoclonal MC-21 antibody results in the suppression of CNV (Liu et al., 2013). The same study reports an enhanced expression of vascular endothelial growth factor in microglia cells accumulated in the lesions sites compared to adjacent RPE cells. It has not yet been clarified whether microglia contribute to the overall VEGF production but their drift towards sprouting vessels is associated with an exacerbation of experimental CNV (Combadiere et al., 2007; Karlstetter et al., 2015).

### 1.2.5 Microglia as therapeutic targets

The previous section 1.2.4 mentioned the multifaceted contribution of microglia cells to AMD. Limiting the disease-driven destructive changes by targeting microglia may therefore decelerate the progression of degeneration (Schuetz and Thanos, 2004). There is growing interest on modulating microglial reactivity towards a regulatory, homeostatic cell phenotype due to their frequent involvement in those neurodegenerative processes. According to this, one strategy to prevent degeneration is to counter-regulate the harmful microglia over-activation with immunomodulatory pharmaceuticals. These include for example the antibiotic minocycline that has also potent anti-inflammatory capacity or the translocator protein (18 kDA) (TSPO) ligand XBD173 (Scholz et al., 2015b,a). Furthermore, natural compounds like the polyunsaturated fatty acid docosahexaenoic acid (DHA), the flavonoid luteolin or the turmeric component curcumin have been shown to modulate microglia gene expression profiles towards an anti-inflammatory phenotype without complete blockade of their functions (Ebert et al., 2009; Dirscherl et al., 2010; Karlstetter et al., 2011). Microglia targeting with such compounds may dampen the production of diverse proinflammatory mediators, eventually inhibiting the damaging microglial reactivity. Also the identification of protective endogenous proteins and their mechanisms of action are valuable findings, potentially providing new strategies for neuroprotection (Aslanidis et al., 2015; Karlstetter et al., 2010; Cardona et al., 2006).
In conclusion, the common aim of these therapeutic strategies is rather to modulate the microglial mode of action to keep its beneficial homeostatic properties than completely preventing the microglia response (Karlstetter et al., 2015).

## 1.3 Type I interferons

Type I interferons (IFN) were discovered more than 50 years ago by Isaacs and Lindenmann as body own signaling molecules inhibiting virus replication in cell culture (Isaacs and Lindenmann, 1987). They belong, next to chemokines, interleukins, tumor necrosis factors and colony stimulating factors, to the large cytokine family (Tilg and Diehl, 2000). Acting on regulatory cell surface glycoproteins they transmit intracellular signaling and communication mechanisms (Tracey and Cerami, 1993). IFNs are especially released in response to viruses, bacteria, parasites, other cytokines and growth factors triggering the protective immune defense (Parkin and Cohen, 2001).
The family of IFNs includes 13 different interferon proteins subdivided in three

groups: Type I IFN, Type II IFN and IFN-like cytokines (Pestka et al., 2004). This thesis concentrates exclusively on the type I interferon IFN-$\beta$.

### 1.3.1 Interferon-beta

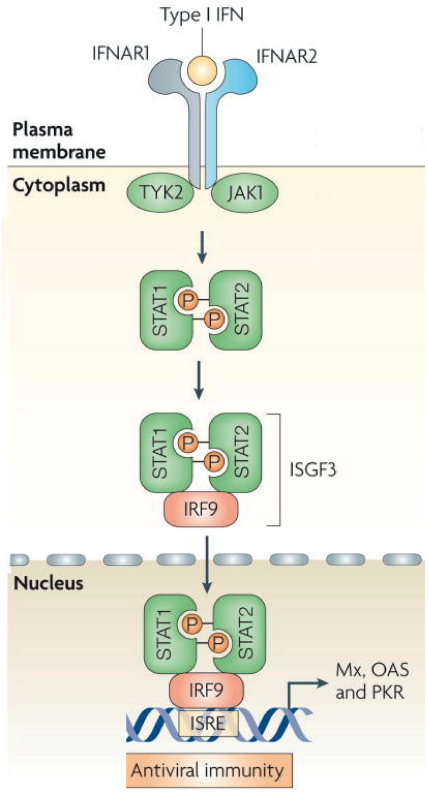


**Figure 1.4:** Activation of the JAK-STAT pathway. Type I interferon IFN-$\beta$ binds to the Interferon-$\alpha/\beta$ receptor and activates the Janus kinase-signal transducer and activator of transcription pathway. IFNAR1- and IFNAR2 associated TYK2 and JAK1 phosphorylate STAT1 and STAT2, which in result heterodimerize forming together with IFR9 the interferon-stimulated gene factor 3. This complex translocates into the nucleus and activates the transcription of interferon-stimulated genes by binding the interferon-stimulated response element. (Scheme modified from Sadler and Williams, 2008).

Interferon beta (IFN-$\beta$) is one out of seven type I interferons (Pestka et al., 2004) and particularly recognized as a key regulator of the innate immune system (Sadler and Williams, 2008). The IFN-$\beta$ gene contains no introns and is in mammalian species encoded by one single gene located on chromosome 9 in humans, coding for a pleiotrophic protein of 166 amino acids (reviewed in Pestka et al., 1987).
IFN-$\beta$ transcription is initiated in response to different transcription factors mainly the interferon regulatory factors (IRF) and then secreted by the cell. Any infected

nucleated cell is capable to produce IFNs (Pestka et al., 2004) but IFN-$\beta$ is predominantly produced by precursors of dendritic cells and fibroblasts (Foster et al., 2000; Stark et al., 1998).
IFN-$\beta$ interacts as type I IFN with the Interferon-$\alpha/\beta$ receptor (IFNAR), a heteromeric cell surface receptor, in an auto- as well as paracrine manner (Uze et al., 2007) and activates the classical JAK-STAT pathway (Fig. 1.4). IFNAR is composed of two subunits, IFNAR1 and IFNAR2, which are associated with Tyrosine kinase (TYK) 2 and Janus kinase (JAK) 1, respectively. Signaling downstream, signal transducer and activator of transcription (STAT) proteins 1 and 2 become phosphorylated by TYK2 and JAK1 and form a heterodimer. The heterodimer associates with a DNA binding protein (IFR-9) and forms a complex called IFN-stimulated gene factor 3 (ISGF3). After formation, the ISGF3 complex translocates into the nucleus and binds to the IFN-stimulated response element (ISRE), which is located upstream of IFN stimulated genes (ISG) and regulates their transcription (reviewed in Bekisz et al., 2004).
There are more than 300 different ISGs induced by IFNAR-signaling mediating biological effects involved in immunity, differentiation, proliferation, apoptosis and angiogenesis. However, only a few interferon-induced genes have direct anti-viral, anti-proliferative or immunomodulatory effect. Instead, other effector pathways like the Mx GTPase pathway, 2'5'oligoadenylate-synthetase-directed ribonuclease L (OAS RNaseL) pathway or the protein kinase R (PKR) pathway have been identified to transduce the IFN-$\beta$-induced mode of action (reviewed in Sadler and Williams, 2008; Friedman, 2008).

### 1.3.2 IFN-$\beta$ as therapeutic agent

Based on their anti-viral, anti-proliferative and immunomodulatory properties IFN-$\beta$ have been used for different clinical applications since the early 1970s. Soon after their discovery by Isaacs and Lindenmann in 1957, it was the antiviral activity of interferons that made them to promising antiviral drugs. IFN-$\alpha$ was used with success to treat chronic hepatitis B virus (HVB) and hepatitis C virus (HVC (Cooksley, 2004; Shepherd et al., 2000). In 1983, Fiblaferon (Rentschler) was the first approved anti-viral drug on the market.
Soon after type I interferon application showed anti-tumor effects in mice, experiments to treat human tumors including renal cancers (Quesada et al., 1983), malignant melanomas (Krown et al., 1984), lymphomas, and leukaemias (Louie et al., 1981) came up (Gresser and Bourali, 1970). Due to the anti-angiogenic effect

mediated by IFNs, the proliferation rate of the tumor cells was attenuated. Roferon A (Roche), the first cancer drug was launched 1987.
Of note, interferon was rare and expensive until 1980s and clinical investigations have been limited. Since the use of recombinant DNA technologies, there are two main variants of recombinant IFN. IFN-$\beta$-1a is produced by mammalian Chinese hamster ovary (CHO) cells, whereas IFN-$\beta$-1b is purified from genetically modified Escherichia coli cultures. As a consequence, IFN-$\beta$-1a is essentially identical to the natural IFN-$\beta$ due to its glycosylation pattern, while IFN-$\beta$-1b differs from the native protein structure (Taniguchi et al., 1980) .
The first steps to clinically use the immunomodulatory properties of IFN-$\beta$ did Jacobs et al. in 1982 (Jacobs et al., 1982). IFN-$\beta$ was administered intrathecally to ten MS patients and then the clinical course was monitored and compared to untreated MS patients for two years. This was the first time a beneficial effect of IFN-$\beta$ on disease progression of MS was shown. Shortly after, IFN-$\beta$ became the first line treatment for relapsing-remitting MS, when Betaseron (Bayer) was launched in 1993.
However, the exact mechanisms of action remain unclear. There are indications that IFN-$\beta$ shapes the T-cell function by regulating their activity, proliferation and migration (Yong et al., 1998). Furthermore, it may modulate the cytokine production profile towards an anti-inflammatory milieu, which is thought to reduce the neuronal inflammation (Kieseier, 2011). Finally, IFN-$\beta$ may inhibit the proliferation of leukocytes and modify their antigen presentation pattern (Yong et al., 1998).
There are several adverse effects induced by IFN-$\beta$ as the endogenous protein is produced in order to fight infections. The temporary increase of cytokine expression causes typical flu-like symptoms, muscle pain, depression, leukopenia, lymphopenia, injection-site reactions and inflammation (Nikfar et al., 2010).
As described in section 1.3.1, the biological function of IFN-$\beta$ is mediated by the expression of ISGs. Of these known functions, the immunomodulatory properties of IFN-$\beta$ are considered to be the most relevant transmitting the therapeutic action in MS.

### 1.3.3 Effect of IFN-$\beta$ on microglia

While section 1.2.2 delineates the contribution of microglia cells to neurodegenerative as well as inflammatory diseases, the purpose of this section is to elucidated the influence of IFN-$\beta$ particularly on microglia cells, the main effector cells of the

innate immune system. In 1997, Chabot and colleges could show in cell culture studies that IFN-$\beta$ modulates the interaction between activated T-lymphocytes and microglia cell, resulting in a reduced production of the proinflammatory cytokine TNF-$\alpha$ (Chabot et al., 1997). Beyond that, an *in vivo* study revealed attenuated experimental autoimmune encephalomyelitis (EAE), a model disease for multiple sclerosis, with excessive microglia activation in mice lacking the IFN-$\beta$ gene (Teige et al., 2003). Prinz and colleagues could show a similar correlation of IFN-$\beta$ and the disease severity of EAE: Animals without IFNAR expression developed provoked clinical disease symptoms characterized by higher inflammation, demyelination and lethality of the mice. While the IFN-$\beta$ concentration in the CNS was increased during EAE, the absence of IFNAR on myeloid cells caused impaired disease symptoms.
Furthermore, the results of recent studies point towards a pivotal role of IFN-$\beta$-signaling during neurodegenerative autoimmune diseases. *In vivo* studies revealed that endogenous IFN-$\beta$ is mainly produced and secreted by microglia cells, which are additionally associated with the clearance of myelin debris (Kocur et al., 2015). Also the endogenous induction of IFN-$\beta$ secretion by intrathecal administration of polyinosinic-polycytidylic acid (poly I:C), had a protective effect during EAE (Khorooshi et al., 2015).
So far, there is little known about the regulation of IFNAR-signaling. A recent study describes ubiquitin-specific protease (USP) 18, an interferon-stimulated gene, as negative regulator of the IFNAR signaling pathway attenuating microglia activation. USP18 terminates the IFNAR-signaling by deactivating Stat1 proteins and therewith inhibiting interferon-induced gene expression (Goldmann et al., 2015).
While the functional results indicate a protective role of IFN-$\beta$ during cerebral inflammation, the precise mode of action of IFN-$\beta$ on microglia remains unclear. Along with that, the question arises whether the results are readily transferable to retinal microglia and neurodegenerative conditions. Therefore, the leading topic of this thesis is the relation between microglia activation and IFN-$\beta$ signaling during AMD-like retinal degeneration.

## 1.4 Aim of the thesis

It is generally accepted that microglia reactivity as well as pathological angiogenesis are deconstructive events in the wet form of AMD promoting degenerative processes leading sooner or later to irreversible vision loss. Thus, understanding the disease formation on the one hand and attenuating excessive immune response on the other hand display a promising strategy to diminish disease burden.

It is postulated that a lack of IFNAR signaling in experimental autoimmune encephalomyelitis, a murine model disease for the cerebral disorder multiple sclerosis (MS), intensifies disease symptoms accompanied by a higher inflammation, demyelination and lethality. Furthermore, IFN-$\beta$ treatment is used as immunomodulatory drug treating MS in humans, without entirely understanding its mode of action.

Therefore there were two aims in this study:

1. Investigating the influence of IFNAR signaling on angiogenesis and microglia reactivity in the retina, both typical hallmarks of AMD pathogenesis, using the laser coagulation model in constitutive and conditional Ifnar1 knock out mice.

2. Analyzing the potential immunomodulatory effect of IFN-$\beta$ on disease symptoms by treating laser coagulated mice with IFN-$\beta$.

# 2 Material and Methods

# 2.1 Material

## 2.1.1 Antibodies and Stains

Table 2.1: List of primary and secondary antibodies as well as other staining reagents used for the experiments.

**Table 2.1:** Antibodies and Stains

| **Antibody & Stain** | **Solution** | **Manufacturer, Article #** |
|---|---|---|
| anti-Iba1, rabbit | 1:500 | Wako; 01-1074 |
| anti-IFN-$\alpha$R1 (MAR1-1H5), mouse | 1:500 | Santa Cruz; sc-53590 |
| GAPDH (I-19), goat | 1:1000 | Santa, Cruz; sc-48166 |
| Alexa Flour 488 (goat anti-rabbit) | 1:1000 | Thermo Fisher; A-11008 |
| Alexa Flour 594 (goat anti-mouse) | 1:1000 | Thermo Fisher; A-11005 |
| IgG-HRP (goat anti-mouse) | 1:2500 | Santa Cruz; sc-2005 |
| IgG-HRP (rabbit anti-goat | 1:2500 | Santa Cruz; sc-2768 |
| DAPI | 0.1 $\mu$g/ml | Invitrogen; D1306 |
| TRITC-Lectin | 0.1 mg/ml | Sigma-Aldrich; L5264 |

## 2.1.2 Enzymes

Table 2.2: List of the used enzymes.

**Table 2.2:** Enzymes

| **Enzyme** | **Manufacturer, Article #** |
|---|---|
| DNAseI, RNase-free | Qiagen, 1010394 |
| RevertAid$^{TM}$ M-MulLV | Thermo Scientifitc, EPO441 |
| Taq Polymerase (PCR) | Genaxxon; M3454 |
| Taq Polymerase (qRT-PCR) | Qiagen; 105476 |
| Proteinase K | Applichem; A3459 |

### 2.1.3 Buffers and Solutions

Table 2.3: List of self-prepared buffers and solutions.

**Table 2.3:** Buffers and Solutions

| Buffer/Solution | Formula |
|---|---|
| 1x Running gel 10% | 3.0 ml 30% Acrylamide, 2.25 ml 1.5 M Tris pH 8.8, 60 $\mu$l 10% APS, 90 $\mu$l 10% SDS, 20 $\mu$l TEMED in 10 ml $dH_2O$ |
| 1x Stacking gel 5 % | 500 $\mu$l 30% Acrylamide, 380 $\mu$l 0.5 M Tris pH 6.8, 32 $\mu$l 10% APS, 32 $\mu$l 10% SDS, 6 $\mu$l TEMED in 3 ml $dH_2O$ |
| 10x DNA loading buffer | 10mM Tris-HCL (pH 7,5), 5 mM Sodium Acetate, 2 mM EDTA 10% Glycerin, 0,001% Bromphenol blue, 0,001% Xylencyanol |
| 10x Running buffer | 29.0 g TRIS, 144.0 g Glycine, 10.0 g SDS in 1 liter $dH_2O$ |
| 10x Transfer buffer | 144.0 g Glycine, 30 g TRIS in 1 liter $dH_2O$ |
| 10x TBE | 1 M Tris, 1 M boric acid, 20 mM, EDTA (pH7.5) in $dH_2O$ |
| 10x TBS-T | 24.2 g TRIS, 80.0 g NaCL, 10 ml Tween-20 in 1 liter $dH_2O$ |
| 30% Sucrose | 30% Sucrose in $dH_2O$ |
| Antibody blocking solution | 2% BSA, 0.2% NaN3, 0.1% Triton X-100 in 1x PBS |
| Agarose gel | 1.5% Agarose in 1x TBE buffer |
| BLOTTO | 1% milk, 0.1% Tween 20 in 1xPBS |
| DAPI solution | 0.1 $\mu$g in 1x PBS |
| Permeabilization buffer | 5% Triton X-100, 5% Tween 20 in 1x PBS |
| RIPA buffer | 150 mM NaCl, 1% NP-40, 0.5% Na-DCA, 0.1% SDS, 50 mM Tris-HCL pH 7.4, 2 mM PMSF, Protease Inhibitor in 10 ml $dH_2O$ |

### 2.1.4 Cell culture and qRT-PCR primers

Tables 2.4: Lists of all cell lines, cell culture reagents and media as well as qRT-PCR probes and primer pairs used for the experiments.

**Table 2.4:** Cell culture consumables

| **Cell line** | **Origin** |
|---|---|
| BV-2 | Prof. Dr. Lucius; Blasi et al. (1990) |
| SV40 | Reiner et al. (2015) |
| **Cell culture reagent** | **Manufacturer, Article #** |
| DMEM High Glucose | Sigma-Aldrich, D5796 |
| Fetal calf serum (FCS) | Gibco, 10270-106 |
| Interferon beta (human) | AbD Serotec, PMP28Z |
| Interferon beta (murine) | PBL; 12400-1 |
| L-glutamin | Gibco, 25030-024 |
| Penicillin/Streptomycin | Gibco, 15140-122 |
| RPMI 1640 medium | Gibco, 31870 |
| **Cell culture media** | **Formula** |
| BV-2 medium | RPMI 1640 medium, 2mN L-glutamin, 1% Penicillin/Streptomycin, 5% FCS and 0.01% $\beta$-Mercaptoethanol |
| SV40 medium | DMEM High Glucose, 10% FCS and 10% Penicillin/Streptomycin |

Table 2.5: List of Roche Library probe numbers and primer pairs used for qRT-PCR .

**Table 2.5:** Probes and Primers for qRT-PCR

| Gene | Probe # | Primer | Sequence |
|---|---|---|---|
| Atp5b | #77 | F | 5'-ggcacaatgcaggaaagg-3' |
| | | R | 5'-tcagcaggcacatagatagcc-3' |
| GAPDH | #60 | F | 5'-gcccaatacgaccaaatcc-3' |
| | | R | 5'-agccacatcgctcagaca-3' |
| MX1, human | #79 | F | 5'-ttcagcacctgatggccta-3' |
| | | R | 5'-aaagggatgtggctggagat-3' |
| Mx1, murine | #53 | F | 5'-ttcaaggatcactcatacttcagc-3' |
| | | R | 5'-gggaggtgagctcctcagt-3' |
| Mx2, murine | #11 | F | 5'-cagttcctctcagtcccaagat-3' |
| | | R | 5'-tgcggttgtgagcctctt-3' |

### 2.1.5 Kit systems, Reagents and Chemicals

Tables 2.6 and 2.7: Lists of used kit systems, reagents and chemicals.

**Table 2.6:** Kits and Reagents

| Kit & Reagents | Manufacturer, Article # |
|---|---|
| DNeasy Blood & Tissue Kit | Qiagen; 69504 |
| NucleoSpin® RNA Mini Kit | Macherey-Nagel; 740955 |
| RevertAid™ RT Kit | Thermo Scientific; K1691 |
| SuperHot Taq PCR Kit | Genaxxon; M3306 |
| SuperSignal West Pico Chemiluminescent Substrate | Thermo Scientific; 34079 |
| dNTP Mix, 10 mM each | Thermo Scientific; R0132 |
| FastStart Universal Probe Master | Roche; 14943600 |
| Fluorescent Mounting Medium | Dako; 53023 |
| GeneRuler 1kb DNA Ladder | Thermo Scientific; SM0311 |
| PageRuler Protein Ladder | Thermo Scientific; 26616 |
| Protease Inhibitor | Roche; 11697498001 |
| Roti®-Quant (Coomassie Brilliant Blue-G250) | Roth; K0151 |
| TissueTek O.C.T. compound | Hartenstein; TTEK |

**Table 2.7:** Chemicals

| Chemical | Manufacturer, Article # |
|---|---|
| 30% Acrylamide | Roth; A124.1 |
| Agarose | Biozym; 84004 |
| Ammonium persulfate (APS) | Sigma-Aldrich; A3678 |
| $\beta$-Mercaptoethanol | Sigma-Aldrich; M-7154 |
| Boric acid | Sigma-Aldrich; B6768 |
| Bromphenol blue | Sigma-Aldrich; B-6131 |
| Bovine Serum Albumin (BSA) | Sigma-Aldrich; A9418 |
| Dimethyl sulfoxide (DMSO) | Sigma-Aldrich; D5879 |
| Disodium phosphate ($Na_2HPO_4$) | Merck; 106566 |
| Ethanol | AppliChem; A3678 |
| Ethidium bromide | Applichem; A0822 |
| Ethylenediaminetetraacetic acid (EDTA) | Sigma-Aldrich; E9884 |
| Glycine | Applichem; A3561 |
| Goat serum | Abcam; ab7481 |
| Isopropanol | Merck; 100995 |
| Methanol | Chemsolute; 1437.2511 |
| NP-40 | Calbiochem; 492016 |
| Paraformaldehyde (PFA) | Sigma-Aldrich; P6148 |
| Phosphate buffered saline (PBS) | Amaresco; E404 |
| Phenylmethylsulfonyl fluoride (PMSF) | Applichem; A0999,0005 |
| Phenylephrin 2.5%/ Tropicamid 0.5% | Pharmacy Uni Clinic Cologne |
| Powdered milk | Roth; T145.3 |
| Sodium azide ($NaN_3$) | Roth; 4221 |
| Sodium chloride (NaCl) | Sigma-Aldrich; S9888 |
| Sodium deoxycholate | Sigma-Aldrich; D6750 |
| Sodium dodecyl sulfate | Roth; CN30.3 |
| Sucrose | Merck; 1.07651 |
| TEMED | Roth; 2367.1 |
| TRIS | Roth; 4855.3 |
| Triton X-100 | Sigma-Aldrich; X100 |
| Tween-20 | Sigma-Aldrich; P1379 |
| Xylencyanol | Sigma-Aldrich; X-4126 |

### 2.1.6 General consumables

Table 2.8: All basic consumables used for the experiments.

**Table 2.8:** General consumables

| Consumable | Manufacturer, Article # |
|---|---|
| 1 ml syringe | BD Plastipak™ |
| 5 ml syringe | BD Discardit™ |
| 1.5 ml cups | Sarstedt; 72.690 |
| 2 ml cups | Sarstedt; 72.689 |
| 15 ml Falcon tube | Sarstedt; 62.554.502 |
| 20G needle | BD Microlance™ 3 |
| 30 $\mu$l pipette tips | Matrix; 7432 |
| 50 ml Falcon tube | Sarstedt; 62.554.254 |
| 6-well culture dish | Sarstedt; 83.3911.002 |
| 96-well plate | Sarstedt; 82.1581.001 |
| Microtome Blades C35 TYPE | Feather |
| Cell scraper | Sarstedt; REF 83.1830 |
| Cryomoldes | Tissue-TEK®; 4557 |
| Cover glasses 18x18mm | Th.Geyer GmbH |
| Biophere® filter tips | Sarstedt; 70.762.217 - 211 |
| Gloves | Braun; 9205926 |
| Lancet | Feather, No.11 |
| MicroAmp Optical 384-well plate | Applied Biosystems; 4326270 |
| MicroAmp Optical adhesive films | Applied Biosystems; 4311971 |
| Superfrost® PLUS microscope slide | Fisher Scientific, 12-550-15 |
| Pasteurpipetten | Sarstedt; 86.1172.001 |
| Pipette tips | Sarstedt; 70.760.002 |
| PCR stripes | Biozym; 711030 |
| T75 culture flask | Sarstedt; 83.3911.002 |

### 2.1.7 Mouse Models

Tables 2.9, 2.10 and 2.11: Mouse models, genotyping primer pairs and injection solutions used for the experiments.

**Table 2.9:** Mouse strains

| Mouse strain | Origin | Reference |
|---|---|---|
| C57BL/6J | own breeding | Dr. CC Little, 1921 |
| Cx3cr1$^{CreER}$ | Prof. Dr. Prinz | (Yona et al., 2013) |
| Ifnar1$^{-/-}$ | Prof. Dr. Kalinke | (Muller et al., 1994) |
| Ifnar1$^{flox/flox}$ | Prof. Dr. Kalinke | (Detje et al., 2009) |
| R26tomato reporter | Prof. Dr. Wunderlich | (Soriano, 1999) |

**Table 2.10:** Primers and PCR programs for Genotyping

| Mouse strain | Primer sequence & PCR program |
|---|---|
| Cx3cr1$^{CreER}$ | forward 5'-cctctaagactcacgtggacctg-3'(wt)<br>forward 5'-gccgcccacgaccggcaaac-3' (tg)<br>revers 5'-gacttccgagttgcggagcac-3'<br>Predenaturation: 5 min 94°C ǀ Denaturation/ Annealing/<br>Elongation: 35x 30 sec 94°C, 45 sec 58°C, 45 sec 72°C ǀ<br>Final elongation: 5 min 72°C |
| Ifnar1$^{-/-}$ | forward 5'-aagatgtgctgttcccttcctctgctctga-3'<br>revers 5'-attattaaaagaaaagacgaggcgaagtgg-3'<br>Predenaturation: 5 min 94°C ǀ Denaturation/ Annealing/<br>Elongation: 35x 30 sec 94°C, 45 sec 58°C, 45 sec 72°C ǀ<br>Final elongation: 5 min 72°C |
| Ifnar1$^{flox/flox}$ | forward 5'-caggccactctgcatttcctc-3' (wt)<br>forward 5'-ctttttggatatcaagaaagcaaat-3' (tg)<br>revers 5'-ctttttggatcgatccataacttcg-3'<br>Predenaturation: 3 min 94°C ǀ Denaturation/ Annealing/<br>Elongation: 35x 30 sec 94°C, 30 sec 58°C, 30 sec 72°C ǀ<br>Final elongation: 5 min 72°C |
| Exon Δ10 | forward 5'-ggttaagctccttgctgctatctgg-3'<br>revers 5'-ttggagatgcaatctgctactcagc-3'<br>Predenaturation: 4 min 94°C ǀ Denaturation/ Annealing/<br>Elongation: 40x 30 sec 94°C, 30 sec 58°C, 2 min 72°C ǀ<br>Final elongation: 10 min 72°C |

**Table 2.11:** Injection solutions

| Injection solution | Manufacturer, Article # |
|---|---|
| 0.9% NaCl | Fresenius Kabi, 06605514 |
| Corn oil | Sigma-Aldrich; C8267 |
| Fluorescein 10% | Alcon, Novartis |
| Interferon beta (human) | AbD Serotec, PMP28Z |
| Ketavet (ketaminehydrochloride) | Pfizer Animal Health |
| Tamoxifen | Sigma-Aldrich; T5648 |
| Rompun (Xylazinhydrochlorid) | Bayer HealthCare |

### 2.1.8 Software and Devices

Tables 2.12 and 2.13: Lists of the main software and devices needed for experiments.

**Table 2.12:** Software

| Software | Manufacturer |
|---|---|
| AlphaEaseFC™ | Alpha Innotech |
| CSl Adobe Creative Suite | Adobe Systems |
| EndNote X7 | Thomson Reuters |
| GraphPad PRISM 6 | GraphPad Software, Inc. |
| Spectralis HRA+OCT Software | Heidelberg Engineering |
| Intas GDS 3.39 sofware | IntasScience Imaging |
| LaTeX | Leslie Lamport, LaTeX Project Team |
| ImageJ | Wayne Rasband, NIH |
| Office Suite | Microsoft Corporation |
| RQ Manager 1.2.1 | Applied Biosystems |
| SDS 2.3 | Applied Biosystems |
| Zen 2012 | Zeiss |

**Table 2.13:** Devices

| Device | Manufacturer |
|---|---|
| 7900 HT Fast Real-Time PCR System | AB Applied Biosystems |
| Adventurer™ Pro balance | Ohaus® |
| ApoTome.2 | Zeiss |
| AxioCam ICc 1 camera | Zeiss |
| AxioCam MRm camera | Zeiss |
| Centrifuge 5415 R | Eppendorf |
| Centrifuge Mini Star | VWR International |
| Cryostat CM3050 | Leica |
| Explorer® Ex 124 balance | Ohaus® |
| Imager.M2 microscop | Zeiss |
| Intas Gel iX20 Imager | Intas |
| Infinite F200 Pro plate reader | Tecan |
| Neubauer counting chamber | OptikLabor |
| HERAcell 240I incubator | Thermo Scientific |
| Heraeus Labofuge 400 R | Thermo Scientific |
| HRA+OCT Spectralis | Heidelberg Engineering |
| MSC-Advantage hood | Thermo Scientific |
| NanoDrop 2000 Spectrophotometer | Thermo Scientic |
| Ophthalas® 532 EyeLite™ Laser | Alcon® |
| peQSTAR 2x cycler | peQlab |
| See-saw rocker SSL4 | Stuart® |
| Thermomixer compact | Eppendorf |
| TissueLyser LT | Qiagen |
| Vortex-genie® | Scientific Industries™ |

## 2.2 Methods

### 2.2.1 Mice

#### 2.2.1.1 Mouse husbandry

The animals used for this work were housed in an air-conditioned environment at 22 $°C$ on a 12 hours light-dark schedule and had access to phytoestrogen-free food and water *ad libitum*. Tail tips were obtained with an age of 21 days and PCR analysis was used to determine the genotype of the animals. The health status of the animals was monitored on a regular basis and all experiments were approved by the governmental body responsible for animal welfare in the state of North Rhine-Westphalia (Landesamt für Natur, Umwelt und Verbraucherschutz Nordrhein-Westfalen, Germany) with the permission number Az 84-02-04-2014-A466.
Ifnar1$^{-/-}$ (Muller et al., 1994), Ifnar1$^{flox/flox}$ (Detje et al., 2009) and R26tomato reporter (Soriano, 1999) mice were on C57BL6/J background, whereas Cx3cr1$^{CreER}$ (Yona et al., 2013) were on C57BL6/N background.
The required animals were sacrificed by cervical dislocation.

#### 2.2.1.2 Genotyping

For DNA extraction the mouse tail tips were digested with proteinase K at 56$°C$ for 4 hours. The DNA was precipitated with isopropanol, then washed with 70% ethanol and dissolved in 100 $\mu$l purified water.

**Genotyping** the mice was performed with polymerase chain reaction (PCR), a standard method to amplify DNA (Kleppe et al., 1971). For that purpose template DNA was mixed with forward and revers primers, taq DNA-polymerase, deoxynucleotide triphosphates (dNTPs) and 10x PCR buffer containing 15 mM $MgCl_2$. A PCR is a cyclic reaction and divided in three steps: denaturation, annealing and elongation. The denaturation causes the disassociation of the DNA double strand by disrupting its hydrogen bonds. During the annealing phase, the respective primers hybridize to the single stranded DNA so that the DNA-polymerase in a third step elongates the primers according to the template DNA. The used primer pairs and PCR programs are listed in Table 2.10.

**Gel electrophoresis** was used to separate the amplified DNA according to its molecular weight. A 1.5% agarose gel was prepared by solving agarose in TBE buffer and 10 $\mu$l ethidium bromide was added before the gel polymerized to visualize the DNA. After PCR, the DNA was mixed with DNA loading buffer and loaded together with

a 1 kb DNA ladder on the gel. 120 V were applied to the gel and the DNA, which is negatively charged, run towards the positive pol.
As ethidium bromide intercalates in DNA, UV light was used to **visualize** the DNA fragments. The agarose gel was documented using a Intas gel documentation station equipped with the Intas GDS 3.39 sofware.

#### 2.2.1.3 Tamoxifen administration

To induce the Cre recombinase activity, Ifnar1$^{flox/flox}$:Cx3cr1$^{CreER}$ and respective control mice were treated with 4 mg tamoxifen dissolved in 200 $\mu$l corn oil. The solution was injected two times subcutaneously at intervals of two days.

#### 2.2.1.4 Interferon beta treatment

The animals were treated with recombinant human interferon beta 1a, produced in CHO cells with a dose of 10,000 Units diluted in phosphate-buffered saline (PBS). 100 $\mu$l of the solution were injected i.p. every other day from day 0 until either day three, seven or 14.

#### 2.2.1.5 Anesthesia

For anestheisa, 150 $\mu$l ketamine hydrochloride (final concentration: 100 mg/kg) and Xylazinhydrochlorid (final concentration: 5 mg/kg) diluted in 0.9% sodium chloride were injected intraperitoneally (0.1 ml per 10 g body weight).

#### 2.2.1.6 Laser-coagulation

The experiments were conducted with 6 to 10 weeks old animals. For laser-coagulation of the retina a slit lamp mounted diode laser system was used. To enlarge the insight into the retina, Phenylephrin 2.5% - Tropicamid 0.5% was applied on the cornea of the animals dilating their pupils. Three laser spots with a single spot size of 100 $\mu$m were induced to both retinas of the animals with an energy level of 125 mW and a duration of 100 ms. The laser spots were applied at 9, 12 and 3 o'clock of the retina and the formation of a bubble indicated the rupture of Bruch's membrane.
The animals were randomly divided into groups and examined after three, seven or 14 days.
This method was performed in cooperation with PD Dr. Albert Caramoy.

#### 2.2.1.7 Fundus fluorescein angiography

For fundus fluorescein angiography (FFA) the animals were again anesthetized and the pupils were dilated. 100 $\mu$l of 2.5% fluorescein diluted in 0.9% sodium chloride was injected intraperitoneally. Infrared and fluorescent pictures were taken by using the Spectralis™ HRA device of the Spectralis™ HRA+OCT 10 min after injection.

**Analysis of FFA**

The choroidal neovascularization was quantified by measuring the mean pixel intensity of the fluorescent leakage per eye. The fluorescence in two regions of interest (ROI) within and one ROI outside every single laser spot was measured using the image processing program ImageJ. The single values were averaged and background fluorescent was subtracted so that one value per eye represented the relative vascular leakage.

Retinas with fused lesion sites or a fusion between lesion site and optical nerve head (ONH) as well as eyes with hemorrhage caused by the laser administration were excluded from analysis.

This method was performed in cooperation with PD Dr. Albert Caramoy.

#### 2.2.1.8 Spectral domain optical coherence tomography

Spectral domain optical coherence tomography (SD-OCT) was performed with anesthetized and pupil-dilated animals. Per scan were 24 images recorded with 40,000 A-scans per seconds and a wavelength of $\lambda$=870 nm using the SD-OCT function of the Spectralis™ HRA+OCT.

To analyze the edema formation in the laser spots the retinal thickness was measured using the software of the Spectralis™ HRA+OCT provided by Heidelberg Engineering.

This method was performed in cooperation with PD Dr. Albert Caramoy.

### 2.2.2 Histological methods

#### 2.2.2.1 Cryo sectioning

Enucleated eyes were first fixated with 4% paraformaldehyde for four hours and then dehydrated in 30% succrose over night. Subsequently, eyes were embedded in TissueTek O.C.T., quick-frozen on dry ice and stored at -80°$C$. 14 $\mu$m thick cryo sections were cut with a CryoMicrotom and mounted on Menzel Superfrost® PLUS microscope slides. The cross sections were stored at -80°$C$ before further use.

#### 2.2.2.2 Flat mount preparation

The enucleated eyes fixated in 4% paraformaldehyde for four hours before the retina and RPE/choroid were separated by using a micro stitch scissors. The tissue was washed and stored in 1x PBS before further processing.

#### 2.2.2.3 Staining of cryo sections

The cryo sections were thawed at room temperature and rehydrated with distilled water for 10 minutes. In a next step, section were blocked with BLOTTO for 1 hour and incubated with the primary antibody or lectin at $4°C$ overnight. The section were covered with Parafilm, a plastic paraffin film, to avoid dehydration. Samples were then washed three times with 1x PBS and incubated with the corresponding secondary antibody for 1 hour at room temperature, again followed by three washing steps. The nuclei were stained with 0.1 $\mu$g/ml DAPI for 10 minutes at room temperature. Before mounting, section were three times washed and then embedded with Dako fluorescent mounting medium.
The primary antibodies were diluted in antibody-blocking solution and the secondary antibodies were diluted in 1x PBS.
The used primary and secondary antibodies and their dilutions are listed in table 2.1.

#### 2.2.2.4 Staining of flat mounts

In a first step, prepared and fixed retinal and RPE/choroidal tissue was permeabilized in a 5% Triton-X/ 5% Tween-20 dilution on a shaker at $4°C$ over night. Followed by the same staining and embedding procedure described in the section above. The nuclei in retinal as well as RPE/choroidal flat mounts were left unstained.

#### 2.2.2.5 Fluorescence microscopy

The images were acquired with an Imager.M2 microscope equipped with ZEN software at 5x or 20x magnification. For the recording of z-stack images, the embedded ApoTome.2 device was used.

**Analysis of images**
The number of round-shaped activated microglial cells was counted within a region of 200 $\mu$m diameter around the laser spot. Microglia morphology was analyzed using a grid system to determine grid crossing points per cell (Chen et al, 2012). CNV areas in RPE/choroidal flat mounts were quantified with the spline function of the graphic tool of ZEN software.

## 2.2.3 Cell culture

### 2.2.3.1 Maintaining and subculturing cells

The murine BV-2 (Blasi et al., 1990) and the human SV40 (Reiner et al., 2015) cell lines were cultured in T75 flasks at 37°$C$ and 5% $CO_2$ humidity. BV-2 cells were culture in RPMI, whereas SV40 cells were cultured in DMEM Gigh Glucose medium. The used cell culture media are listed in table 2.4. Both cell lines were split every second day in a ration one to three by scratching them off the flask bottom and transferred in a new cell culture flask provided with new medium.

### 2.2.3.2 Interferon beta stimulation

For IFN-$\beta$ stimulation 100.000 cell were transferred in a 6-well plate one day before stimulation started and stimulated with 1000 U/ml human or murine IFN-$\beta$ for 24 hours. Before harvesting the RNA, cells were washed with 1x PBS.

## 2.2.4 Molecular methods

### 2.2.4.1 RNA isolation

For RNA purification the silica-membrane technology of the NucleoSpin® RNA Kit was used. Therefore, the old culture medium was discarded, the cells were washed with 1x PBS and subsequently lysed with the provided RA1 lysis buffer. Following isolation steps were carried out according to the manufacturer's protocol. Finally, the RNA was eluted with 40 $\mu$l nuclease-free water and stored at -80°C until further processing.

### 2.2.4.2 Determination of RNA concentration

The RNA concentration and purity was measured spectrophotometrically using a NanoDrop 2000 device. For quantification, the absorbance at 260 nm and 280 nm was measured and the concentration was calculated using the Beer-Lambert law ($E_\lambda = \varepsilon \cdot d \cdot c$ with E = extinction at wavelength $\lambda$, $\varepsilon$ = molar extinction coefficient, d = thickness of sample and c = concentration of sample). RNA with an A260/280 ratio of 2.0 or higher was considered as pure and used for experiments.

#### 2.2.4.3 Reverse transcription

For real time PCR analysis single stranded RNA needs to be rewritten into double-stranded also referred as complementary DNA (cDNA). The synthesis of 1 $\mu$g RNA was performed using the RevertAid™ RT Kit according to the manufacturer's protocol.

#### 2.2.4.4 Quantitative real-time PCR

The quantitative real-time PCR (qRT-PCR) is based on the PCR but additionally monitors the amplification of targeted DNA sequences via a fluorescence signal. To increase the specificity of qRT-PCR, the TaqMan technology was used (Holland et al., 1991). This method uses probes carrying a fluorophore linked reporter at the 5' end and a quencher at the 3' end, which are complementary to the targeted DNA sequence. The fluorescence emitted by the fluorophore in response to a light stimulus is inhibited as long as fluorophore and quencher are in close proximity to each other. Once the Taq polymerase synthesizes the cDNA strand, the probes, which are annealed to the target sequence, become degraded. This process causes the release of the fluorophore and abrogates its close proximity to the quencher allowing fluorescence of the fluorophore. The fluoresence intensity increases exponentially with every PCR cycle and is equivalent to the amount of DNA sample applied for PCR.
The analysis was performed in 10 $\mu$l reaction mixtures containing 50 ng cDNA (2.5 $\mu$l), 5 $\mu$l 2x TaqMan Gene Expression Mastermix, 200 nM forward and reverse primers (1 $\mu$l each), 0.125 $\mu$l fluorescent-labeled probe and 0.375 $\mu$l nuclease-free water. Roche Library Probe numbers and primer pairs are listed in table 2.5. The PCR protocol included 40 cycles (Denaturation: 40 sec 95°C, annealing: 60 sec 60°C and elongation: 2 min 72°C) and the results were analyzed with the RQ Manager software using the ΔΔCt method for relative quantification.

**ΔΔCt quantification**
The amount of fluorescence directly depends on the amount of cDNA sample applied during PCR. If the amount of PCR cycles increases the detected fluorescent increases directly proportional. Once the fluorescence intensity crosses a certain threshold, the qRT-PCR device starts recording the amount of cycles needed to reach the threshold. This resulting parameter is referred as Ct (Cycle threshold) value.
The ΔΔCt analysis for quantification of qRT-PCR is a frequently used algorithm to calculate the relative changes in gene expression. It requires, next to the expression

analysis of the gene of interest, the recording of a house keeping gene, which is equally expressed in all samples. The relative expression changes are then determined by comparing the expression levels of both reactions. First, the mean Ct values of the reactions, which are performed in duplicates, are calculated. In a next step, the recorded Ct values are normalized to the house keeping gene. This enables the comparison of relative gene expression between two genes, as the expression level of the house keeper in both samples should be similar. The house keeping gene used for the human cell line was GAPDH and for the murine assay ATPase was used. In a third step, one untreated sample is set to one as calibrator. The Ct values and the relative quantification were determined using the RQ 2.1 Manager software.

The detailed calculation is demonstrated in the following list:

1. Calculation of mean Ct value
   **Ct avg**
2. Nomalization to the house keeper gene
   $\mathbf{\Delta Ct\ avg = Ct\ avg_{gene} - Ct\ avg_{house\ keeper}}$
3. Setting calibrator as reference
   $\mathbf{\Delta\Delta Ct\ avg = \Delta Ct\ avg_{sample} - \Delta Ct\ avg_{calibrator}}$
4. Relative difference of gene expression
   $\mathbf{2^{-\Delta\Delta Ct\ avg}}$

#### 2.2.4.5 Protein isolation

To isolate whole protein, the neuronal retina was homogenized in 50 $\mu$l RIPA buffer using a TissueLyser LT (1 min/, 40/sec). The solved proteins were separated from the remaining tissue by centrifugation for 5 minutes at 5000 g. All steps were performed on ice and RIPA buffer and centrifuge were previously cooled down to avoid protein degradation.

#### 2.2.4.6 Determination of protein concentration

The protein concentration was measured spectroscopically by using Bradford assay (Bradford, 1976). This method is based on an spectral absorbance shift as the red form of Coomassie Brilliant Blue G-250 dye changes into it its bluer form when attached to proteins. The more protein binds, the bluer the dye. For Bradford assay

the Roti®-Quant solution was used according to the manufacture's protocol and the spectral absorption was monitored using a Tecan plate reader equipped with a 595nm filter.

#### 2.2.4.7 Western Blot

Western blotting was used to specifically detect Ifnar1 proteins in tissue samples of homogenized retinas. In a first step, the dissolved proteins were separated by using gel electrophoresis. For this purpose, 30 $\mu$g of each sample were loaded together with a ladder on a 10% SDS-PAGE (sodium dodecyl sulfate - polyacrylamide gel electrophoresis) and 100 V voltage were applied to segregate the proteins according to its molecular weight. In a next step, proteins were transferred to a 0.45 $\mu$m nitrocellulose membrane. After blocking unspecific binding sites with 5% milk powder in 1x PBS for 1 hour, the membrane was incubated with the primary antibody overnight at $4°C$. The membrane was three times washed with TBS-T buffer and incubated with a horseradish peroxidase (HRP)-tagged secondary antibody for 1 hour at room temperature. To visualize the western blot signal SuperSignal West Pico was used as a oxidizing agent and the emerging chemiluminescence was detected with a Multiimage II system.

### 2.2.5 Statistical analysis

The statistical analysis was performed by using the program GraphPad Prism 6. Two diffenrent groups were compared with the unpaired Student's t-test and more than two groups were anlayzed via one-way ANOVA followed by Tukey's post-test. The values presented in this work indicate the mean $\pm$ standard deviation (SD). P-values less than 0.05 were considered as significant.

# 3 Results

## 3.1 Effect of IFNAR knockdown in laser-coagulation model

A previous *in vivo* study showed exacerbated clinical disease symptoms in mice lacking the IFN-$\alpha/\beta$ receptor (Ifnar1$^{-/-}$) during experimental autoimmune encephalomyelitis (EAE), an induced multiple sclerosis model (Prinz et al., 2008). Furthermore, Ifnar1$^{-/-}$ mice developed higher cerebral inflammation, demyelination and lethality compared to controls.
However, since very little was known about the role of IFNAR signaling on age-related macular degeneration (AMD) pathogenesis features such as microglial activation and angiogenesis, the current study sought to fill this gap using a murine laser-coagulation model. All animals were laser-treated at experiment onset and the three key events induced by the model namely microglia activation, vascular leakage and choroidal neovessel formation (CNV) were analyzed 3, 7 and 14 days post laser damage (Fig. 3.1). The earlier time point ensures the detection of activated microglia cells, the intermediate time point showed the clearance of the inflammation and development of the CNV, whereas the late time point captured the ongoing CNV formation and eventual wound healing processes.

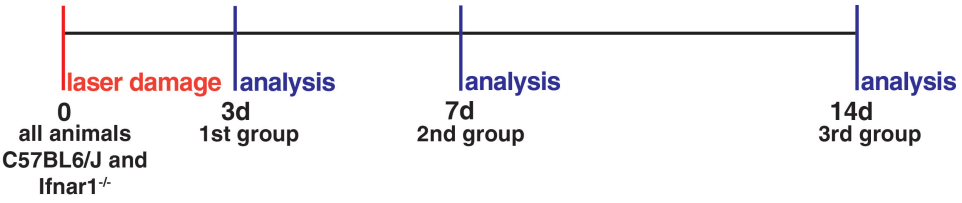


**Figure 3.1:** Experimental Setup. Laser coagulation was performed in Ifnar$^{-/-}$ and C57BL6/J control mice and analyzed 3, 7 and 14 days later. (Figure published in Lueckoff et al. (2016))

### 3.1.1 Microglia activation

To characterize the microglial activation status and their reactivity, retinal and RPE/choroidal flat mounts were performed 3 and 7 days post laser damage.
First, retinal flat mounts were stained with Iba1, a specific marker for microglial cells, to compare the amount and morphology of microglia cells in the laser spot. Analyzing the confocal images of the retinal flat mounts revealed a mixed ramified and amoeboid cell population at the lesion site 3 days post laser damage (Fig. 3.2 A). In contrast, the major population of microglia cells in the laser spots in Ifnar1$^{-/-}$

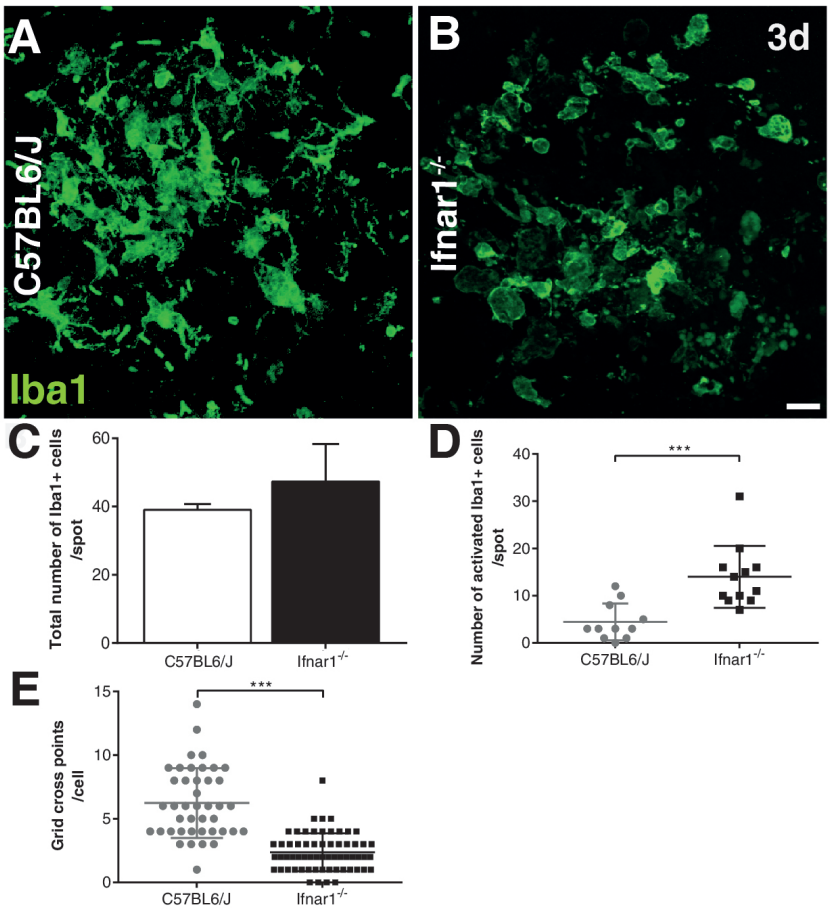


**Figure 3.2:** Immunohistological characterization of microglia cells in laser spot. Representative confocal images of Iba1 stained retinal flat mounts of C57BL6/J control (A) and Ifnar$^{-/-}$ mice (B) analyzed 3 days post laser treatment. For quantification the total amount (C) and the amount of amoeboid-shaped (D) microglia cells was count. The microglial morphology was analyzed using a grid image analysis system (E). Scale bar: 20 $\mu$m. Values show mean $\pm$ SD. (Total count: n = 3; Amoeboid-shaped: n = 11-12 retinas; Cell morphology: n = 42-62 cells; unpaired Student's t-test; Figure published in Lueckoff et al. (2016))

mice was obviously amoeboid shaped (Fig. 3.2 B).

The quantification of the Iba1 stainings revealed a significantly higher amount of amoeboid microglia cells in mice lacking Ifnar1 (14 $\pm$ 1.9 cells/spot) compared to wild type controls (4.5 $\pm$ 1.2 cells/spot) (Fig. 3.2 D, ***p $\leq$ 0.0004), pointing towards a more reactive cell population. The total number of microglial cells within the laser spots did not significantly differ in both groups of animals (Fig. 3.2 C)

Also a grid cross analysis, elaborating the morphological constitution of the microglial cells by counting the number of crossing points per cell, showed less grid cross points in Ifnar1$^{-/-}$ mice compared to controls (2.4 $\pm$ 0.2), identifying highly activated microglia cells. In contrast, the microglia cells in C57BL6/J wild type had

6.2 $\pm$ 0.4 grid crossing points per cell (Fig. 3.2 E, ***p $\leq$ 0.0001). These results indicate a strong influence of Ifnar1-deficiency shifting the cell morphology in the affected tissue towards an amoeboid, reactive phenotype.

### 3.1.2 Fluorescein leakage

In a next step we investigated whether the IFNAR signaling has an influence on the severity of the laser-induced neovessel formation. To capture that, the late phase of the fluorescein leakage was measured by fundus fluorescein angiography (FFA) as a parameter for choroidal neovascularization at an early, intermediate and late time point (Fig. 3.3 A-F). Ifnar1-deficiency had no major effect on the vascular leakage at day 3 and 7. Remarkably, significant differences in vascular leakage were detected 14 days post laser damage with Ifnar1$^{-/-}$ animals exhibiting enhanced leakage when compared to wild type controls (Fig. 3.3 G, ***p $\leq$ 0.0001).

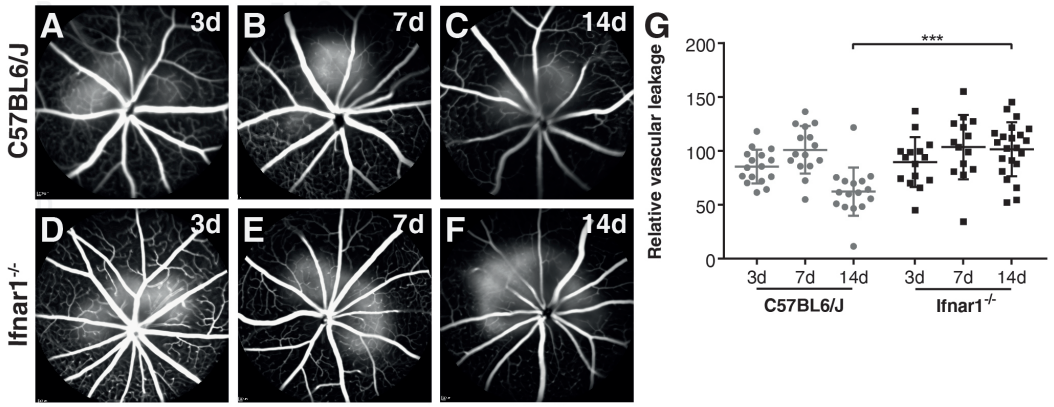


**Figure 3.3:** Fundus fluorescein analysis of retinal leakage. The fluorescent leakage in C57BL6/J and Ifnar$^{-/-}$ mice was compared using late phase fluorescent images. (A-F) Representative images of both groups 3, 7 and 14 days post laser treatment. (G) Quantification of vascular leakage by analyzing pixel intensity. Values show mean $\pm$ SD. (n = 14-22 eyes; One-way ANOVA followed by Tukey's post-test; Figure published in Lueckoff et al. (2016)).

### 3.1.3 Choroidal neovascularization

To image the CNV size histologically, retinal pigment epithelia was stained with lectin (Fig. 3.4 A-D). Ifnar-deficient animals showed significant increased total CNV area 14 days after laser damage when compared to the wild type control animals (Fig. 3.4 E, *p $\leq$ 0.0281).

Furthermore, retinal cross sections analyzed at day 3 revealed an increased amount of microglia cells in the subretinal space co-labeled with lectin in Ifnar1$^{-/-}$ mice compared to wild type controls (Fig. 3.5 A, B).

In addition, flat mounted retinas and RPEs at day 7 post laser damage revealed notably more reactive Iba1 labeled microglia cells in the laser spots and the subretinal space of Ifnar1 deficient mice (Fig. 3.6 A, B). Together, these findings indicate that a constitutive loss of Ifnar1 signaling provokes a higher accumulation of reactive microglia cells in the site of damage and an enlarged CNV formation, both enhancing disease severity.

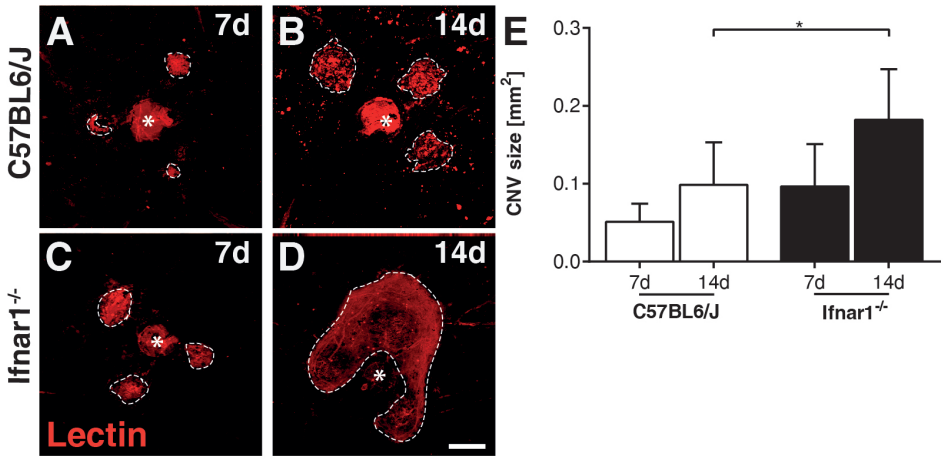


**Figure 3.4:** Choroidal neovascularization in Ifnar$^{-/-}$ and C57BL6/J mice. Retinal pigment epithelium were stained with lectin to label the newly built blood vessels 7 and 14 days post laser treatment. Images of C57BL6/J (A, B) and Ifnar$^{-/-}$ (C, D) mice were quantified by analyzing the stained area (E). Dashed lines indicate CNV areas and the asterisks mark the central optic nerve head. Scale bar: 200 $\mu$m. (n = 4-11 RPE/choroidal flat mounts; One-way ANOVA followed by Tukey's post-test; Figure published in Lueckoff et al. (2016)).

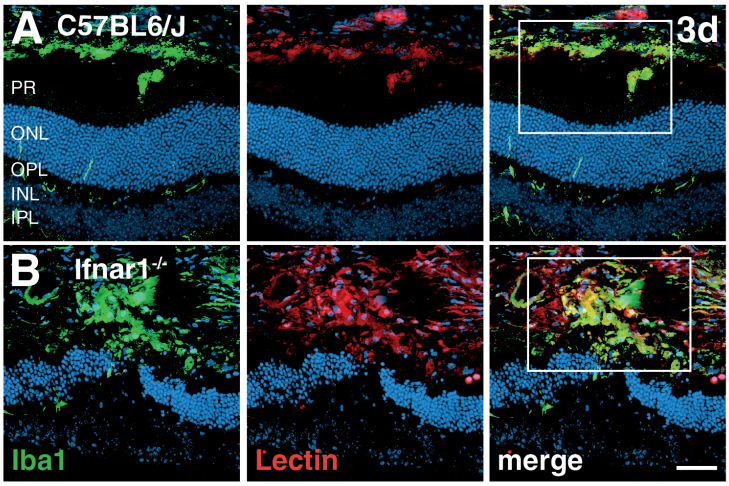


**Figure 3.5:** Immunohistological analysis of microglia accumulation and CNV in the subretinal space. Representative images of Iba1 and lectin co-stained retinal cross sections 3 days post laser treatment in C57BL6/J wild type (A) and Ifnar1$^{-/-}$ (B) mice. The white boxes indicate the spot where the laser hit the retina. Nuclei are DAPI stained. Scale bar: 50 $\mu$m. (Figure published in Lueckoff et al. (2016))

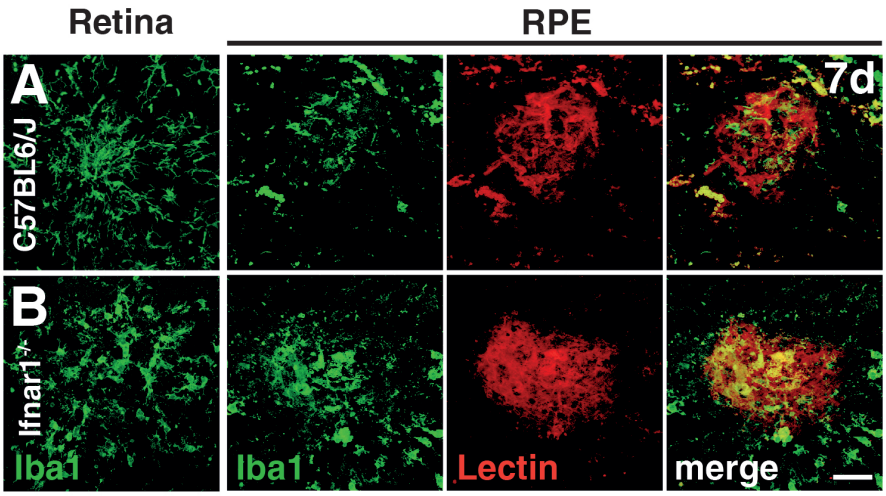


**Figure 3.6:** Immunohistological analysis of microglia accumulation and CNV in the subretinal space. Representative images of Iba1 stained retinal flat mounts and Iba1 and lectin co-stained RPE/choroidal flat mounts 7 days post laser-coagulation in C57BL6/J (A) and Ifnar1$^{-/-}$ (B) mice. Scale bar: 50 $\mu$m. (Figure published in Lueckoff et al. (2016))

## 3.2 The biological activity of human IFN-$\beta$ in murine cells

To pretest the functionality of human IFN-$\beta$ in a murine system, the murine microglia cell line BV-2 was stimulated with 1000 U/ml human IFN-$\beta$ for 24 hours. The expression of two classical IFN-$\beta$ target genes myxovirus resistance 1 and 2 (Mx1 and Mx2) was measured by quantitative real-time PCR (qRT-PCR), the results indicating a 385.3 fold induction of Mx1 and 36.5 fold induction of Mx2 compared to unstimulated cells (Fig. 3.7 A, B), implying good biological activity of human IFN-$\beta$ in a murine cell line.
The biological activity of the human IFN-$\beta$ was also validated using human SV40 immortalized microglia cell line, with similar results on Mx1 induction being achieved (Fig. 3.7 C).

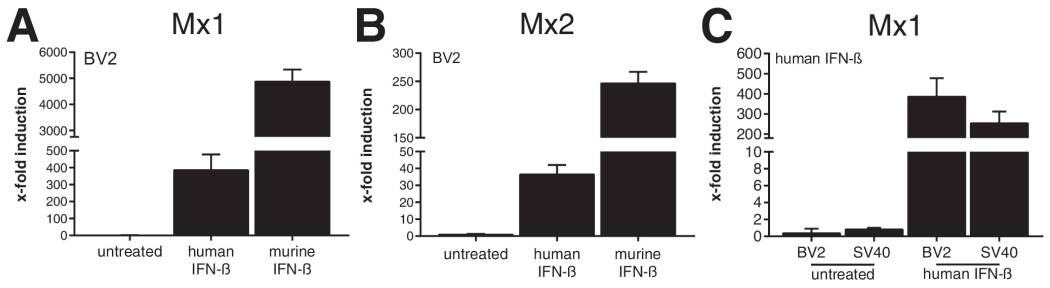


**Figure 3.7:** Testing the bioactivity of human IFN-$\beta$ in murine cell line. Murine BV-2 were stimulated for 24 hours with either human or murine IFN-$\beta$ (A, B). Human SV40 cells were stimulated for 24 hours with human IFN-$\beta$ (C). The expression of the classical IFN-$\beta$ induced genes Mx1 and Mx2 was analyzed using qRT-PCR. (Figure published in Lueckoff et al. (2016)).

## 3.3 Effect of systemic IFN-$\beta$ therapy in the laser-coagulation model

Based on the Ifnar1$^{-/-}$ data set, which demonstrated that disease symptoms were more severe in animals lacking Ifnar1, a potential therapeutic effect of the Ifnar-ligand IFN-$\beta$ during laser induced retinal damage in mice was hypothesized. To test this hypothesis, laser damage was performed in C57BL6/J animals followed by subsequent treatment with 10,000 units human IFN-$\beta$ every other day for 3, 7 or 14 days. Microglial activity, fluorescent leakage and choroidal neovascularization were then analyzed as shown in Fig. 3.8.

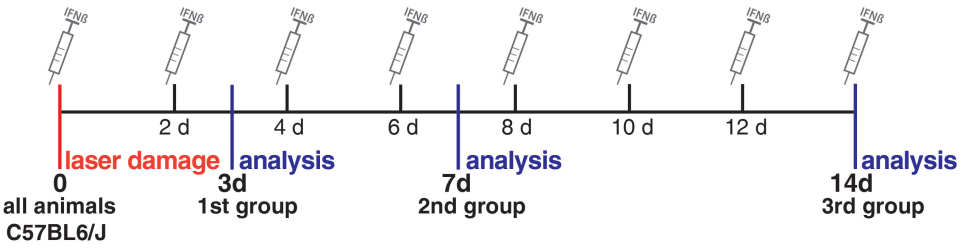


**Figure 3.8:** Experimental Setup. Laser coagulation was performed in IFN-$\beta$ treated C57BL6/J and untreated control mice and analyzed 3, 7 and 14 days later. (Figure published in Lueckoff et al. (2016)).

### 3.3.1 Microglia activation

Changes in the microglial activation status were examined 3 and 7 days post laser damage in flat mounted retinas and RPEs as well as 3 days post laser-coagulation in retinal cross sections by Iba1 staining (Fig. 3.9 A, B). The amount of amoeboid shaped microglia cells was significantly lower in the laser spots of IFN-$\beta$ treated animals compared to untreated C57BL6/J controls (Fig. 3.9 D, ***$\leq$ 0.0003). Indeed, IFN-$\beta$ treated groups showed a highly ramified microglial cell morphology characterized by a small soma and long cellular processes (Fig. 3.9 E, p $\leq$ 0.0001). In addition, the total number of Iba1 positive cells within the laser spots did not change in the IFN-$\beta$ treated group (Fig. 3.9 C).

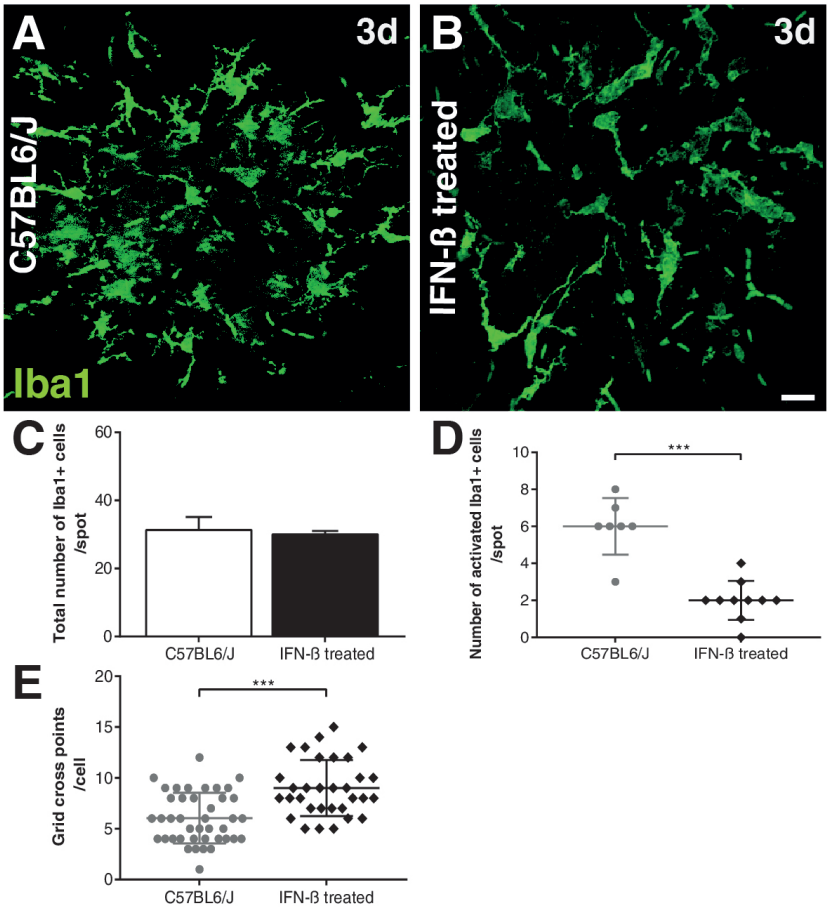


**Figure 3.9:** Immunohistological characterization of microglia cells in the laser spot. Representative confocal images of Iba1 stained retinal flat mounts of untreated C57BL6/J control (A) and IFN-$\beta$ treated C57BL6/J (B) mice analyzed 3 days post laser treatment. For quantification the total amount (C) and the amount of amoeboid-shaped (D) microglia cells was counted. The microglial morphology was analyzed using a grid cross image analysis system (E). Scale bar: 20 $\mu$m. Values show mean $\pm$ SD. (Total count: n = 3; Amoeboid-shaped: n = 7-10 retinas; Cell morphology: n = 42-62 cells; unpaired Student's t-test; Figure published in Lueckoff et al. (2016)).

### 3.3.2 Fluorescein leakage

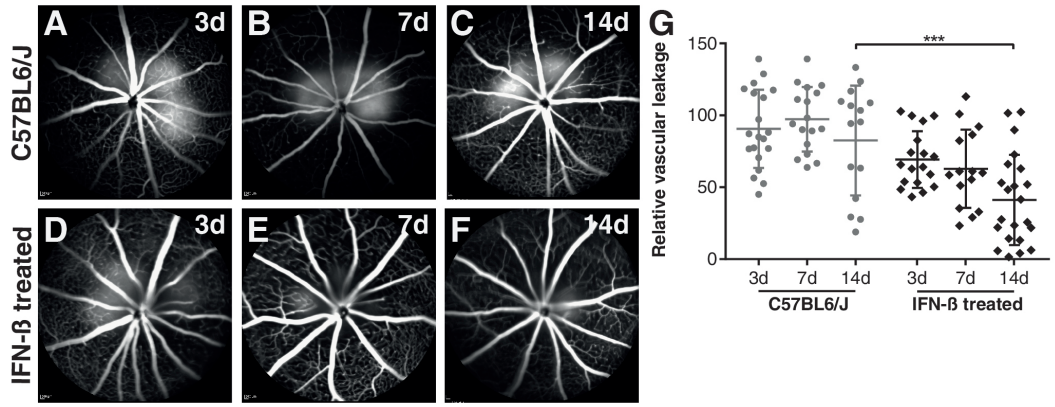


**Figure 3.10:** Fundus fluorescein analysis of retinal leakage. The fluorescent leakage in IFN-$\beta$ treated C57BL6/J and untreated control mice was compared using late phase images. (A-F) Representative images of both groups 3, 7 and 14 days post laser treatment. (G) Quantification of vascular leakage by analyzing pixel intensity. Values show mean $\pm$ SD. (n = 8-12 eyes; One-way ANOVA followed by Tukey's post-test; Figure published in Lueckoff et al. (2016)).

Comparing the vascular leakage 3, 7 and 14 days post laser-coagulation in untreated versus IFN-$\beta$-treated C57BL6/J mice using fundus fluorescent angiography, the IFN-$\beta$ treated groups showed a considerably improved disease course (Fig. 3.10 A-F), as shown by a strong reduction in fluorescent exudate leaking into the retinal tissue (Fig. 3.10 G, ***p $\leq$ 0.0004).

### 3.3.3 Choroidal neovascularization

Histological analysis of the CNV formation by lectin staining revealed that IFN-$\beta$ treatment had a remarkable influence in reducing the total CNV area of the lesion 14 days post laser damage (Fig. 3.11 A-E, **p $\leq$ 0.0038).
Similar results were obtained for the analysis of retinal cross sections at day 3 (Fig. 3.12 A, B) and of retinal and RPE/choroidal flat mounts at day 7 (Fig. 3.13 A, B), with IFN-$\beta$ treated animals exhibiting weaker Iba1-lectin co-staining. These results indicate a less pronounced immune activation with concomitant decrease in CNV formation following IFN-$\beta$ treatment.

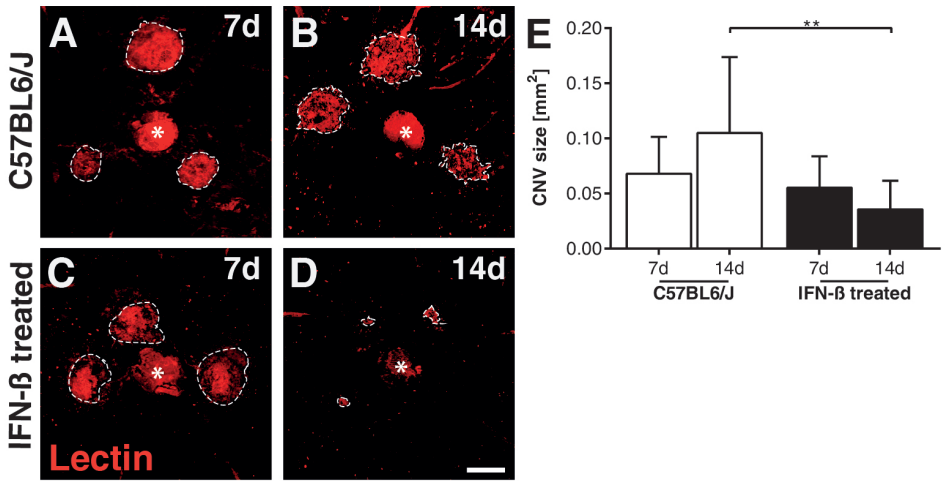


**Figure 3.11:** Choroidal neovascularization in IFN-$\beta$ treated C57BL6/J and untreated control mice. Retinal pigment epithelium were stained with lectin to label the newly built blood vessels 7 and 14 days post laser treatment. Images of untreated C57BL6/J (A, B) and IFN-$\beta$ treated C57BL6/J (C, D) mice were quantified by analyzing the stained area (E). Dashed lines indicate CNV areas and the asterisks mark the central optic nerve head. Scale bar: 200 $\mu$m. (n = 18-22 RPE/choroidal flat mounts; One-way ANOVA followed by Tukey's post-test; Figure published in Lueckoff et al. (2016)).

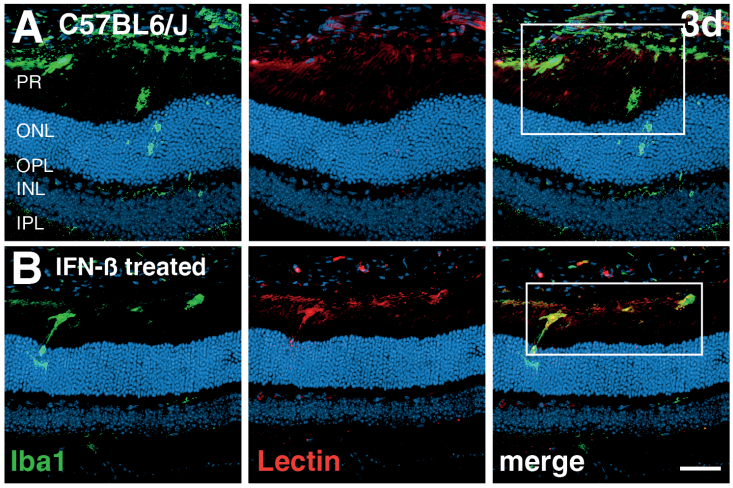


**Figure 3.12:** Immunohistological analysis of microglia accumulation and CNV in subretinal space. Representative images of Iba1 and lectin co-stained retinal cross sections 3 days post laser treatment in untreated C57BL6/J (A) and IFN-$\beta$ treated C57BL6/J (B) mice. The white boxes indicate the spot where the laser hit the retina. Nuclei are DAPI stained. Scale bar: 50 $\mu$m. (Figure published in Lueckoff et al. (2016)).

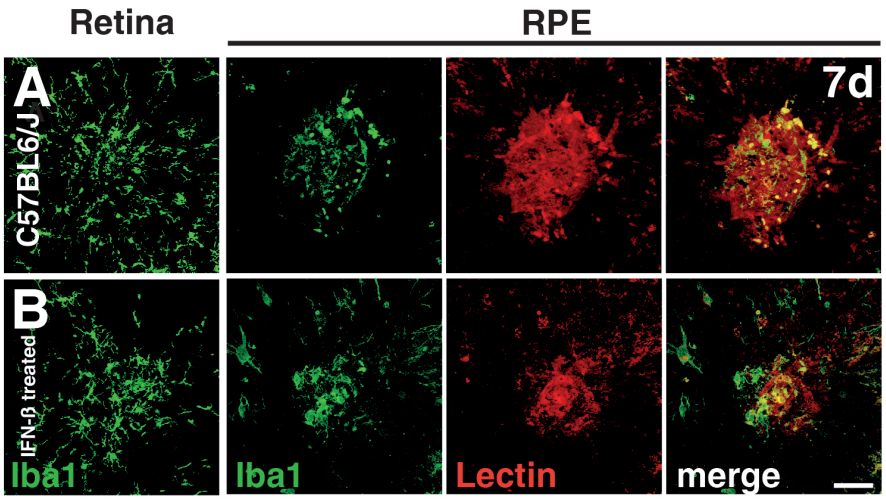


**Figure 3.13:** Immunohistological analysis of microglia accumulation and CNV in subretinal space. Representative images of Iba1 stained retinal flat mounts and Iba1 and lectin co-stained RPE/choroidal flat mounts 7 days after laser coagulation in untreated C57BL6/J (A) and IFN-$\beta$ treated C57BL6/J (B) mice. Scale bar: 50 $\mu$m. (Figure published in Lueckoff et al. (2016)).

### 3.3.4 Edema formation

Following laser administration, interstitial fluid, called edema, often congregates in the subretinal space and thickens the retina. To validate whether IFN-$\beta$ also has an effect on edema formation, the retinal thickness was measured by optical coherence tomography 7 and 14 days after laser damage. OCT analysis of the laser-treated area revealed that IFN-$\beta$ therapy mediated a faster regression of the subretinal edema (Fig. 3.14, *** $p \leq 0.0079$), indicating a supportive wound healing processes.

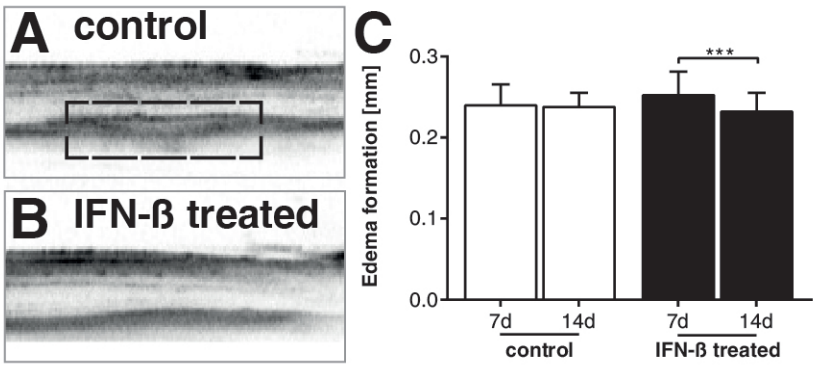


**Figure 3.14:** Edema formation in IFN-$\beta$-treated animals. Representative optical coherence tomography images show the edema in C57BL6/J control (A) and IFN-$\beta$ treated (B) animals. The edema formation was quantified by measuring the retinal thickness 7 and 14 days (C) post laser-coagulation.

## 3.4 Microglia-specific knockdown of Ifnar1

After demonstrating the protective effect of the IFN-$\beta$ therapy, the next aim was to investigate whether the protective effects observed following IFN-$\beta$ therapy and in animals expressing Ifnar versus Ifnar$^{-/-}$ mice were mediated purely by microglia cells or whether other retinal cells are involved in the protective cascade. To test this, experiments were performed using the Cre-Lox system, a genetic tool to generate cell specific knockouts in mice. For that purpose, Ifnar1$^{flox/flox}$ mice, carrying two loxP recognition sites in the Ifnar1 gene, were crossed with Cx3cr1$^{CreER}$ mice carrying a tamoxifen inducible Cre recombinase under the control of the microglia specific Cx3cr1 promoter. Notably, the long longevity and limited self-renewal nature of microglia cells when compared to other myeloid cells enabled the induction of Ifnar1 knockout specifically in microglia cells upon tamoxifen application. The infiltrating myeloid cells with higher turnover rate lose the Cre activity without the activating tamoxifen, which was administered 4 weeks before the laser damage procedure.

### 3.4.1 Microglia specificity of Cx3cr1 controlled Cre recombinase

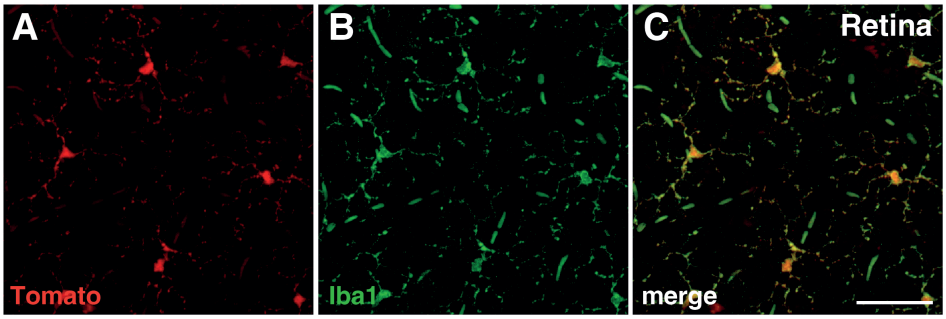


**Figure 3.15:** Cre activity in retinal microglia. Representative images of retinal flat mounts of Cx3cr1$^{CreEr}$:R26$^{tomato}$ mice co-stained with Iba1 four weeks after tamoxifen injection showing microglia specificity of the Cx3cr1-promoter controlled recombinase. The tomato signal (A) and the Iba1 staining (B) co-localize (C) indicating a high recombination efficiency. (Figure published in Lueckoff et al. (2016)).

The microglia specificity of the Cre recombinase was tested by crossing Cx3cr1$^{CreER}$ mice with R26$^{tomato}$ Cre reporter mice and treating them with tamoxifen. Retinal flat mounts of these animals showed a distinct co-localization of the tomato signal with Iba1 staining. This finding indicated a high recombination efficacy in microglial cells (Fig. 3.15 A-C).

### 3.4.2 Specific knockdown of Ifnar1

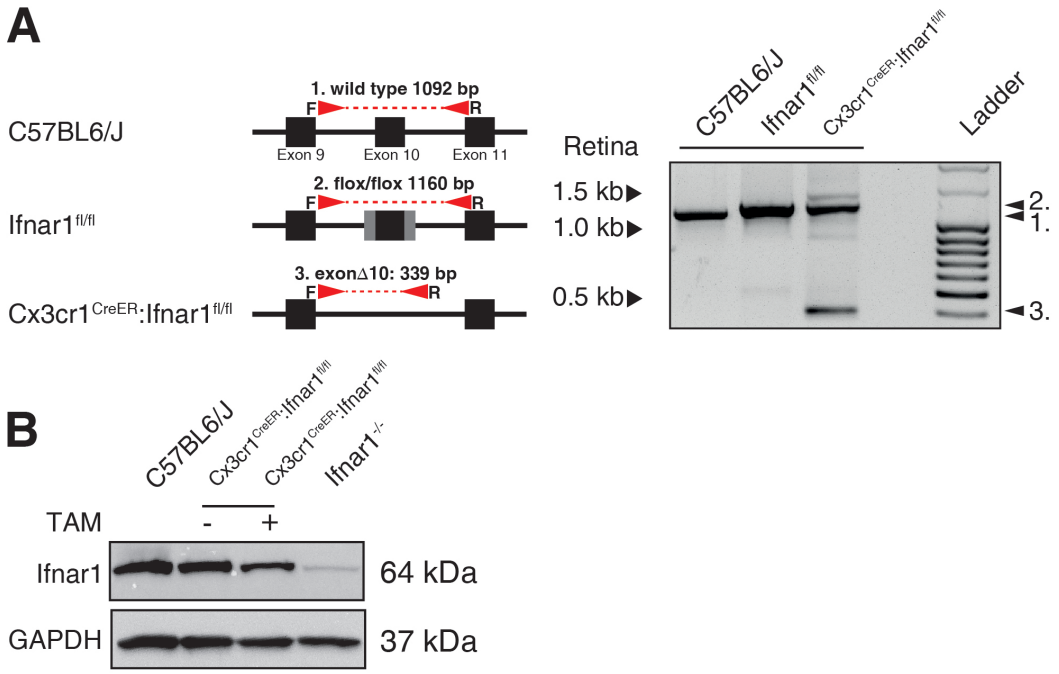


**Figure 3.16:** Knockdown of Ifnar1 in Cx3cr1$^{CreEr}$:Ifnar$^{flox/flox}$ mice. The Ifnar1 gene locus in schematically shown for C57BL6/J wild type, Ifnar$^{flox/flox}$ and tamoxifen treated Cx3cr1$^{CreEr}$:Ifnar$^{flox/flox}$ mice. To confirm the conditional knockout of Ifnar1, PCR analysis were performed with genomic DNA from retina samples. Amplification of a floxed exon 10 resulted in a 1160 bp fragment, while the excision of exon 10 (Δ10) leads to a 339 bp fragment (A). Western blot analysis confirmed reduced Ifnar1 expression in retinal protein extracts of tamoxifen-treated Cx3cr1$^{CreEr}$:Ifnar$^{flox/flox}$ mice (B). (Figure published in Lueckoff et al. (2016)).

In a next step, Cx3cr1$^{CreEr}$:Ifnar1$^{flox/flox}$ mice were generated. To confirm the Cre-mediated excision of exon 10 of the Ifnar1 gene, PCR analysis was performed with genomic DNA from retina samples. The PCR strategy shows the localization of the primer. Amplification and gel electrophoresis of a floxed exon 10 resulted in a 1160 bp fragment, while the excision of exon 10 (Δ10) leads to a 339 bp fragment. A 1092 bp fragment was displayed in C57BL6/J mice carrying no loxP sites (Fig. 3.16 A). Western blot analysis with an antibody directed against Ifnar1 confirmed the reduced Ifnar1 expression in whole retina extracts of tamoxifen treated Cx3cr1$^{CreEr}$: Ifnar1$^{flox/flox}$ mice (Fig. 3.16 B).

Additionally, co-staining of retinal cross sections with antibodies directed against Ifnar1 and Iba1 show no Ifnar1 signal in Ifnar1$^{-/-}$ mice (Fig. 3.17 B) and a weaker Ifnar1 signal in Cx3cr1$^{CreEr}$: Ifnar1$^{flox/flox}$ mice (Fig. 3.17 C). Co-staining the cross

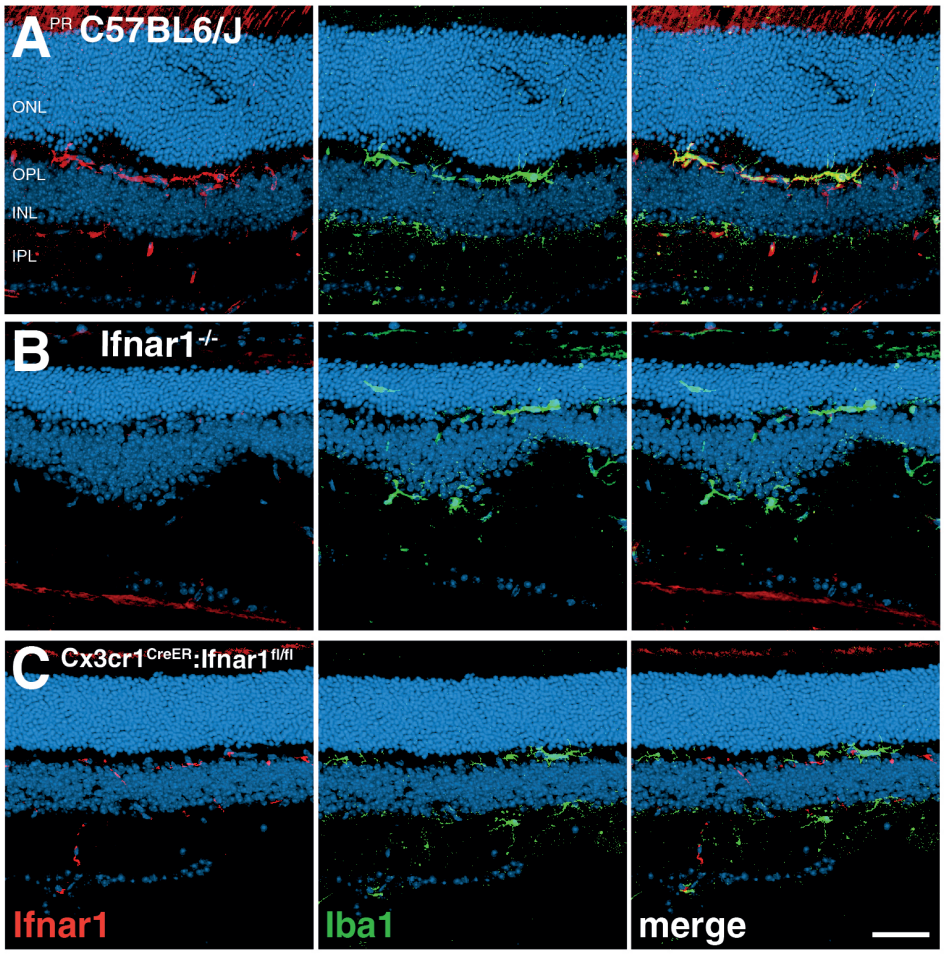


**Figure 3.17:** Immunohistological characterization of Ifnar1 knockdown in C57BL6/J, Ifnar1$^{-/-}$ and Cx3cr1$^{CreEr}$:Ifnar1$^{flox/flox}$ mice. Retinal cross sections were co-stained with antibodies targeting Iba1 and Ifnar1 comparing Ifnar1 expression signal and Iba1 co-localization in C57BL6/J (A), Ifnar1$^{-/-}$ (B) and Cx3cr1$^{CreEr}$:Ifnar1$^{flox/flox}$ (C) animals. (Figure published in Lueckoff et al. (2016)).

section with Iba1 revealed a clear co-localization of both, the Ifnar1 and Iba1 signals in C57BL6/J control animals (Fig. 3.17 A).

## 3.5 Effect of microglia-specific IFNAR knockdown in laser-coagulation model

Laser-induced coagulation experiments were performed with Cx3cr1$^{CreEr}$:Ifnar1$^{flox/flox}$ mice. Cx3cr1$^{CreEr}$ and Ifnar1$^{flox/flox}$ mice carrying either the Cre-recombinase or the floxed Ifnar allele were used as controls. To only target long living microglia cells with a slow turnover rate, mice were injected twice with 4 mg tamoxifen four weeks before starting the experiment. To later compare the results with the previously obtained data sets, the experimental setup was left unchanged (Fig. 3.18).

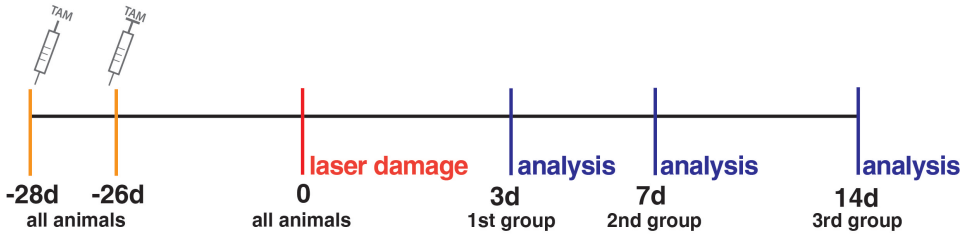


**Figure 3.18:** Experimental setup. Laser coagulation was performed in Cx3cr1$^{CreEr}$: Ifnar1$^{flox/flox}$, Cx3cr1$^{CreEr}$ and Ifnar1$^{flox/flox}$ mice four week after tamoxifen treatment. The animals were analyzed 3, 7 and 14 days later. (Figure published in Lueckoff et al. (2016)).

### 3.5.1 Microglia activation

Retinal microglia lacking Ifnar1 expression displayed a more reactive phenotype compared to Iba1+ cells located into the lesion site from Cx3cr1$^{CreEr}$ and Ifnar1$^{flox/flox}$ mice (Fig. 3.19 A-C), indicating a reactive phenotype.
Also counting the amount of amoeboid microglia cells attested a significantly higher number of activated microglia cell in Cx3cr1$^{CreEr}$:Ifnar1$^{flox/flox}$ mice (Fig. 3.19 E, $^{**}p \leq 0.0044$, $^{***}p \leq 0.0003$), which additionally showed significantly less ramifications in the grid cross analysis system (Fig. 3.19 F, $^{***}p \leq 0.0001$). The total amount of Iba1+ cell did not change after excising Ifnar1 (Fig. 3.19 D).

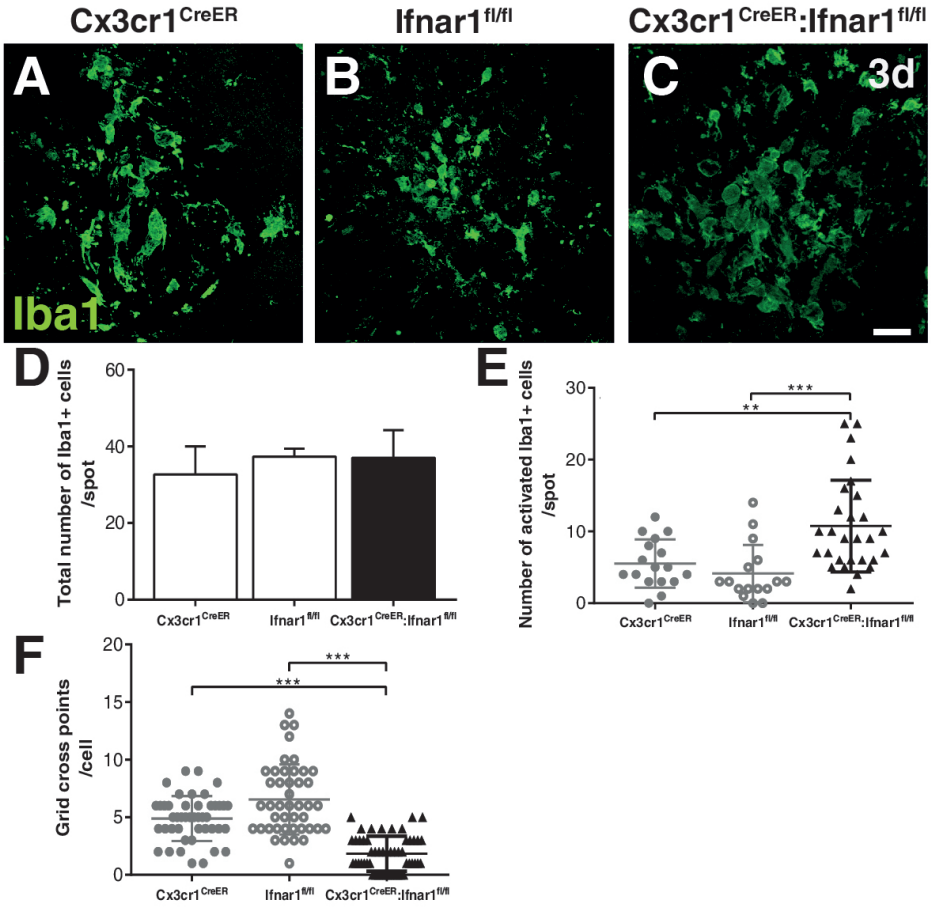


**Figure 3.19:** Immunohistological characterization of microglia cells in the laser spots. Representative confocal images of Iba1 stained retinal flat mounts of Cx3cr1$^{CreEr}$:Ifnar1$^{flox/flox}$ (A), Cx3cr1$^{CreEr}$ (B) and Ifnar1$^{flox/flox}$ (C) mice analyzed 3 days post laser treatment. For quantification the total amount (D) and the amount of amoeboid-shaped (E) microglia cells was counted. The microglial morphology was analyzed using a grid cross image analysis system (F). Scale bar: 20 $\mu$m. Values show mean $\pm$ SD. (Total count: n = 3; Amoeboid-shaped: n = 16-28 retinas; Cell morphology: n = 44-52 cells; unpaired Student's t-test; Figure published in Lueckoff et al. (2016)).

### 3.5.2 Fluorescein leakage

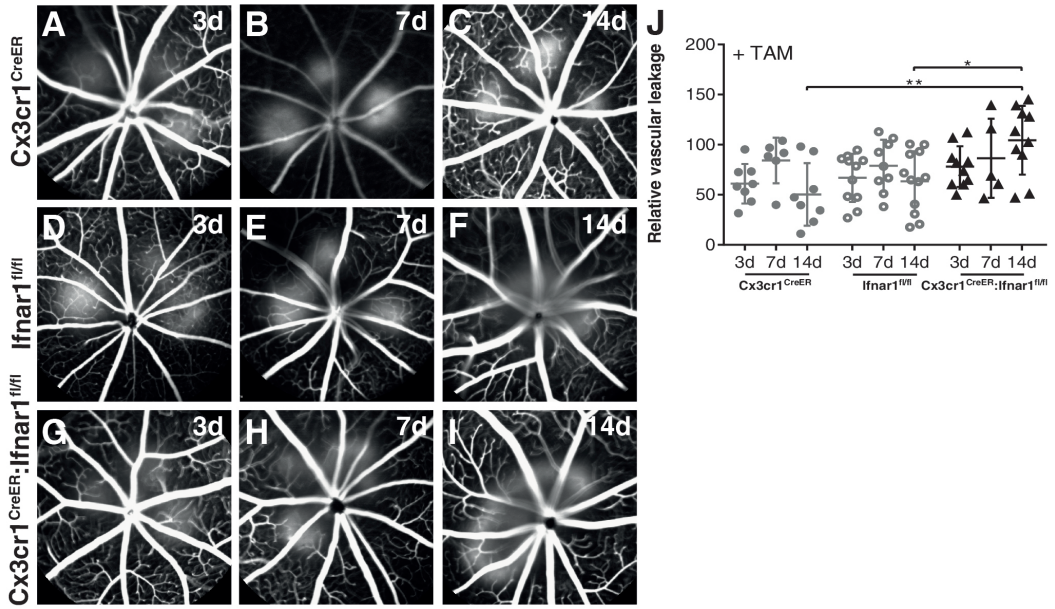


**Figure 3.20:** Fundus fluorescein analysis of retinal leakage. The fluorescent leakage in Cx3cr1$^{CreEr}$:Ifnar1$^{flox/flox}$, Cx3cr1$^{CreEr}$ and Ifnar1$^{flox/flox}$ mice was compared using late phase images. (A-I) Representative images of both groups 3, 7 and 14 days post laser treatment. (J) Quantification of vascular leakage by analyzing pixel intensity. Values show mean ± SD. (n = 5-12 eyes; One-way ANOVA followed by Tukey's post-test; Figure published in Lueckoff et al. (2016)).

The disease progression was monitored by comparing the vascular leakage at day 3, 7 and 14 days post laser treatment (Fig. 3.20 A-I). Cx3cr1$^{CreER}$: Ifnar1$^{flox/flox}$ animals developed, compared to their control counterparts carrying only Cre recombinase or floxed Ifnar1 alleles, a more robust vascular leakage by day 7, reaching its peak after 14 days (Fig. 3.20 J, **p $\leq$ 0.0032 and *p $\leq$ 0.0247).

### 3.5.3 Choroidal neovascularization

Quantification of lectin stained RPE/choroidal flat mounts revealed a significant increase in total CNV area in mice lacking Ifnar1 in microglia cells 14 days after laser treatment, when compared to Cx3cr1$^{CreER}$ and Ifnar1$^{flox/flox}$ controls (Fig. 3.21 A-G, *p $\leq$ 0.043, ***p $\leq$ 0.0007).

Furthermore, the temporal correlation of Iba1 stained microglia with CNV lesions in retinal cross sections at day 3 and RPE/choroidal flat mounts at day 7 in all three analyzed groups (Fig. 3.23 A-C) revealed a clear overlap of amoeboid microglia cells

with increased lectin signal in Cx3cr1$^{CreER}$:Ifnar1$^{flox/flox}$ animals when compared to Cx3cr1$^{CreER}$ and Ifnar1$^{flox/flox}$ controls groups at both time points (Fig. 3.23 A-C). Taken together, these results display an essential role of Ifnar1-signaling in the activation state of microglia and that loss of Ifnar1 enhances the formation of laser-induced CNV lesions.

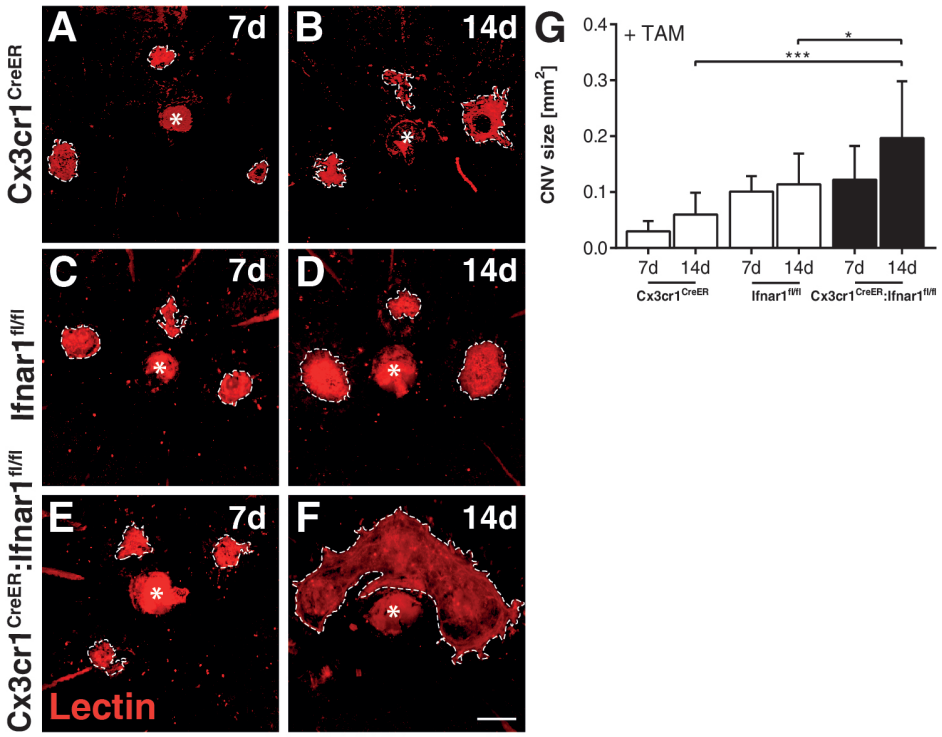


**Figure 3.21:** Choroidal neovascularization in Cx3cr1$^{CreEr}$:Ifnar1$^{flox/flox}$, Cx3cr1$^{CreEr}$ and Ifnar1$^{flox/flox}$ mice. Retinal pigment epithelium were stained with lectin to label the newly built blood vessels 7 and 14 days post laser treatment. Images of Cx3cr1$^{CreEr}$:Ifnar1$^{flox/flox}$ (A,B), Cx3cr1$^{CreEr}$ (C,D) and Ifnar1$^{flox/flox}$ (E,F) mice were quantified by analyzing the stained area (F). Dashed lines indicate CNV areas and the asterisks mark the central optic nerve head. Scale bar: 200 $\mu$m. (n = 10-12 RPE/choroidal flat mounts; One-way ANOVA followed by Tukey's post-test; Figure published in Lueckoff et al. (2016)).

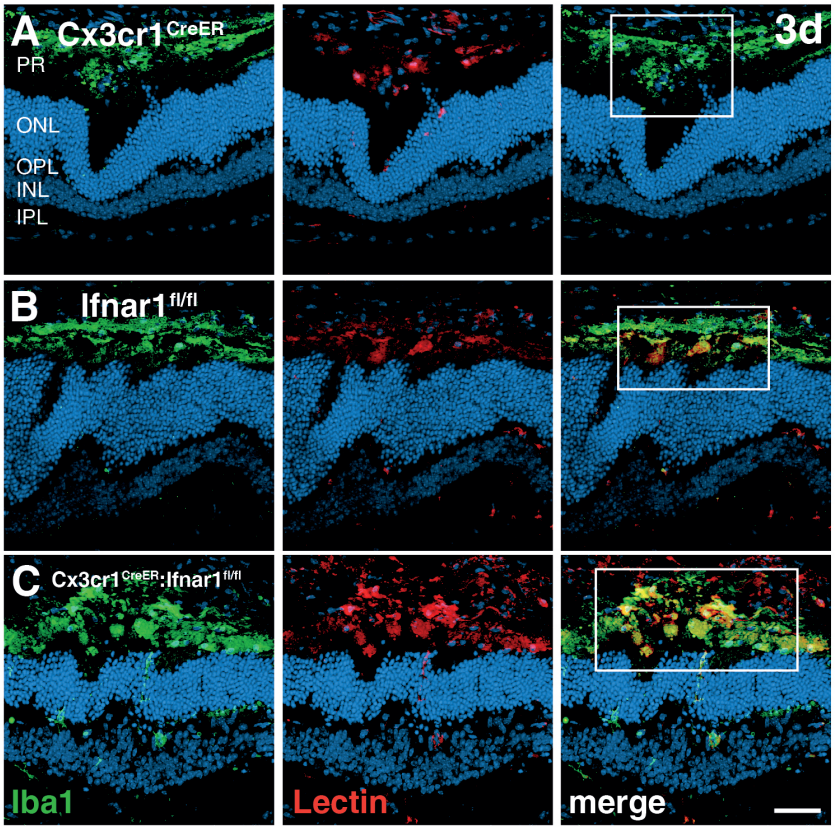


**Figure 3.22:** Immunohistological analysis of microglia accumulation and CNV in the sub-retinal space. Representative images of Iba1 and lectin co-stained retinal cross sections 3 days post laser treatment in Cx3cr1$^{CreEr}$ (A), Ifnar1$^{flox/flox}$ (B) and Cx3cr1$^{CreEr}$:Ifnar1$^{flox/flox}$ (C) mice. The white boxes indicate the spot where the laser hit the retina. Nuclei are DAPI stained. Scale bar: 50 $\mu$m. (Figure published in Lueckoff et al. (2016)).

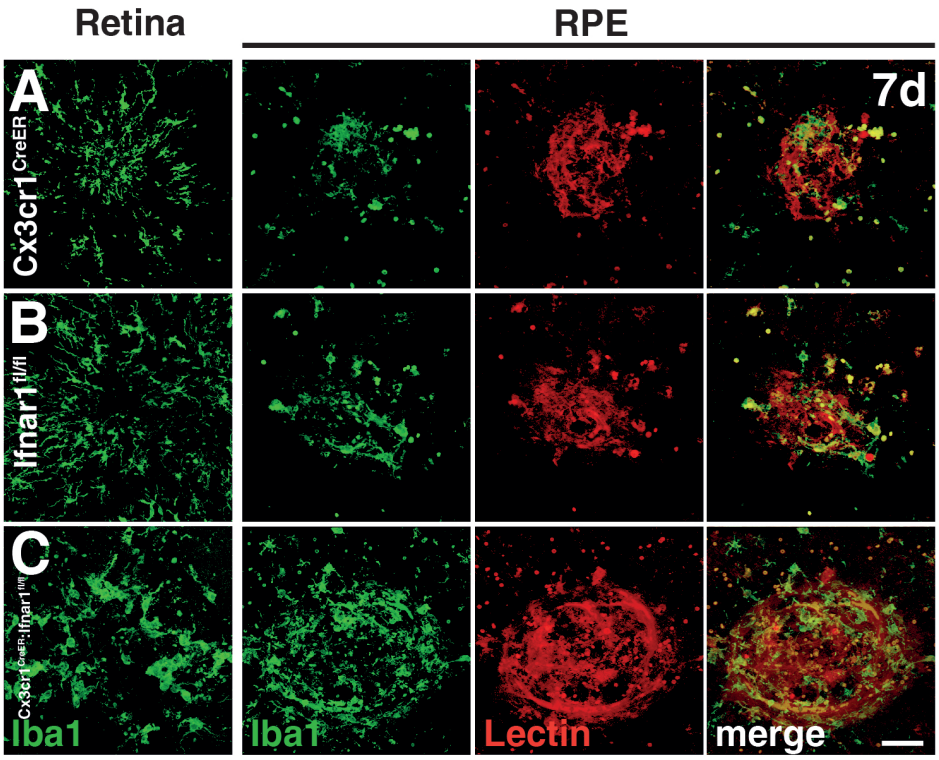


**Figure 3.23:** Immunohistological analysis of microglia accumulation and CNV in the subretinal space. Representative images of Iba1 stained retinal flat mounts and Iba1 and lectin co-stained RPE/choroidal flat mounts 7 days after laser-coagulation in Cx3cr1$^{CreEr}$ (A), Ifnar1$^{flox/flox}$ (B) and Cx3cr1$^{CreEr}$:Ifnar1$^{flox/flox}$ (C) mice. Scale bar: 50 $\mu$m. (Figure published in Lueckoff et al. (2016)).

# 4 Discussion

In this work the influence of type I interferon receptor (IFNAR) signaling on retinal microglia function and angiogenesis in a murine laser-coagulation model was analyzed. The aim was to investigate the potential immunomodulatory effect of IFNAR and IFN-$\beta$ treatment in the pathogenesis and progression of AMD.
It is postulated that a lack of IFNAR signaling in other neurodegenerative disorders such as experimental autoimmune encephalomyelitis (EAE), a murine model disease for the cerebral disorder multiple sclerosis (MS), leads to an intensified disease progression accompanied by a higher inflammation, demyelination and lethality. On the other hand, IFN-$\beta$ is used in humans as an immunomodulatory drug in the treatment of MS, without entirely understanding its mode of action.

## 4.1 Laser-induced photocoagulation as model for wet AMD

Unlike the laser-induced photocoagulation model, age-related macular degeneration (AMD) is a spontaneously appearing and progressive condition caused by several risk factors. These notwithstanding, a lot of insights and knowledge on the disease have been acquired through the use of this well-established experimental model for wet AMD.
Rupturing Bruch's membrane with laser administration enables the ingrowth of blood vessels from the choroid through the Bruch's membrane and into the avascular subretinal space (Lambert et al., 2013). This process initiates both, microgliosis and angiogenesis, two main hallmarks of pathological processes involved in the wet AMD and hence, the use of laser-coagulation model mimics these pathological features of AMD (Tobe et al., 1998).
The suitability of this model is enhanced by the easy accessibility of the retina and the experimental setup which offers the opportunity to administer different potential therapeutic substances or compounds, including neutralizing antibodies, siRNA or drugs via various methods (Saishin et al., 2003; Sabatel et al., 2011; Lueckoff et al., 2016). Consequently, the laser-induced photocoagulation model is frequently used for analyzing the effect of new drugs or therapy targets. Drugs which have been tested using this model include the vascular endothelial growth factor receptor (VEGFR) trap (Saishin et al., 2003), anecortave acetate (Slakter, 2006) and miR-21 a microRNA (Sabatel et al., 2011). While the model is also established in rats and monkeys (Shen et al., 1998; Ryan, 1979), experimenting with mice allows the use of

transgenic animals (Luhmann et al., 2012; Tobe et al., 1998) to elucidate specific molecular mechanisms related to a genetic basis.
This model is however not without limitations. There exist fundamental differences between the model disease and human AMD, limiting the transferability of the experimental results. Mice, which are the preferred species of choice in this model,are used as inbred lines with poor genetic diversity and kept in a pathogen-free environment with constant exterior conditions like temperature and food. This contrasts AMD development in human patients where genetic predisposition as well as nutrition and lifestyle are some of the main risk factors contributing to disease onset (Gong et al., 2015). Moreover, in the current model laser-coagulation is responsible for the formation of microgliosis and CNV (Lambert et al., 2013) as opposed to the aging process of the retinal tissue or other age-dependent changes such as the formation of drusen in human patients.
Furthermore, the induction of the model disease requires a traumatic injury to rupture Bruch's membrane, which provokes a wound-healing reaction relying heavily on inflammation (Lambert et al., 2013; Espinosa-Heidmann et al., 2003; Sakurai et al., 2003). This inflammatory response causes the contribution of inflammatory cells like microglia and macrophages (Liu et al., 2013; Apte et al., 2006) and results in a spontaneous disease regression after approximately 14 days (Lambert et al., 2013). Also compared to AMD, where the disease trigger and course varies from patient to patient, the model displays rather a homogenous disease with little variance between single experimental animals.
Further limitations of the model include the lack of a macula in mice and the requirement of pigmented mice for laser-reactions (Lambert et al., 2013).
However, despite these limitations, the performed experiments were able to show that the laser-coagulation model can be employed to accurately analyze the influence of IFNAR-signaling in retinal microglia following an AMD-like pathogenesis.

## 4.2 The murine and human type I interferon system

In contrast to several new drugs and target options tested directly on murine models like EAE or the laser-induced coagulation model, the therapeutic effect of IFN-$\beta$ was primarily shown in human trials (Paty and Li, 2001). It therefore raises the question whether the effect of IFNAR-signaling observed in mice can be simply transferred to the human situation.

However, the type I interferon system of both species consists of 13 different IFN-$\alpha$ subtypes and one IFN-$\beta$. In humans, additional type I interferons are IFN-$\omega$ and IFN-$\kappa$, both having similar biological functions and bind the same interferon-$\alpha$/-$\beta$ receptor (IFNAR) as other type I interferons (Hardy et al., 2004). In mice, an additional type I IFN has recently been identified and named IFN-like 1 or limitin (Oritani et al., 2000).
IFNAR is a transmembrane receptor consisting of two subunits, IFNAR1 and IFNAR2 (Uze et al., 2007), and transduces extracellular signals into the nucleus by activating the JAK-STAT signaling pathway (Pestka et al., 2004). Humans and mice produce IFN-$\beta$ in a host of different cell types such as fibroblasts, dendritic and microglia cells (Liu, 2005; Kocur et al., 2015). In both these species, anti-viral, anti-tumoral and immunomodulatory activities are related to type I interferon signaling (Friedman, 2008). Indeed, animals lacking IFN-$\beta$ exhibit a spontaneous Parkinson-like neurodegeneration (Ejlerskov et al., 2015), underlining the immunomodulatory role of this cytokine.
Moreover, the similarities in the type I interferon system point towards a comparable function in CNS health of both species so that in this work, the use of human IFN-$\beta$ for treatment experiments seems plausible. Moreover, human IFN-$\beta$ has a great relevance because it is frequently used as human therapeutic compound. In research applications, it has been previously used in murine BV-2 cell assays (Goldmann et al., 2015) and in a CNV model in rabbits (Yasukawa et al., 2002), clearly provoking effects. This is in line with the results of the performed BV-2 and SV40 cell stimulation assays to test the bioactivity of human IFN-$\beta$ in a murine system, before elaborating it's effects on laser-induced microgliosis and CNV (see Fig. 3.7): quantitative RT-PCR showed a comparable upregulation of typical IFN-$\beta$-signaling marker genes Mx1 and Mx2 (myxovirus resistance 1 and 2) in the murine as well as human cell line. Therefore, treating mice with human IFN-$\beta$ caused a significantly ameliorated disease course, which supports the conclusion that IFN-$\beta$ derived from both species mediates similar effects.

## 4.3 The protective effect of IFNAR on laser-induced AMD-like pathology

Ifnar1$^{-/-}$ animals, lacking the Ifnar1 subunit of the receptor (Muller et al., 1994), show a stronger and prolonged disease course, with an elevated accumulation of amoeboid microglia cells at the lesion sites and an increased CNV formation. These results

fully correspond with previous studies reporting that interferon-$\beta$/IFNAR-signaling has immunomodulatory effects on experimental autoimmune encephalomyelitis (EAE), a model for autoimmune brain inflammation and multiple sclerosis (Prinz et al., 2008): Mice lacking Ifnar1 expression developed exacerbated clinical disease symptoms accompanied by higher inflammation, demyelination and lethality (Prinz et al., 2008). This negative influence of Ifnar1-deficiency on EAE was not seen upon Cre-mediated deletion of Ifnar in B-cells or T-cells but was fully recapitulated by LysM-Cre directed deletion of Ifnar in myeloid cells (Prinz et al., 2008). In line with that disrupting the gene of the Ifnar ligand Interferon beta (IFNß) also leads to an augmented and sustained CNS inflammation and demyelination in EAE (Teige et al., 2003).

Microglia evolved from distinct primitive yolk-sac progenitor cell (Kierdorf et al., 2013), are the primary innate immune effector cells in the CNS and are involved in degenerative pathologies of the brain and the retina (Kettenmann et al., 2011; Nimmerjahn et al., 2005; Langmann, 2007; Karlstetter et al., 2015; Zhao et al., 2015).

To specifically analyze the role of Ifnar1 signaling in retinal microglia function, the experiments were repeated using a tamoxifen-inducible Cx3cr1$^{CreER}$ mouse. This mouse model was established to target microglia *in vivo*, facilitating inducible gene deletion in adult animals after tissue and cell maturation (Goldmann et al., 2013; Yona et al., 2013). Beyond that, it is capable of distinguishing microglia cells from other myeloid cells expressing chemokine C-X3-C motif receptor 1 (Cx3cr1) by their longevity and ability of self-renewal, both unique features of microglia (Wieghofer et al., 2015). It remains uncertain if other long-living resident mononuclear phagocyte populations located in proximity to the retina such as choroidal tissue macrophages are also potentially targeted by this system (McMenamin, 1999). Tamoxifen-induced Cx3cr1$^{CreERT2}$:Ifnar1$^{flox/flox}$ mice showed the same significantly enhanced disease pathology like Ifnar1$^{-/-}$ mice compared to controls expressing functional Ifnar1 on microglia cells. Thus, the influence of Ifnar1 signaling on disease formation seems to be primarily mediated by microglia cells, pointing towards a significant contribution of this cell type to increase choroidal neovascularization in the laser-coagulation model.

In addition, unpublished data of our lab revealed typical IFNß-stimulated genes like interferon-related developmental regulator 1 (Ifr1), interferon-induced GTP-binding protein Mx1 (Mx1) and signal transducer and activator of transcription 2 (Stat2) to be upregulated in Rs1h$^{-/y}$ and Fam161a$^{GT/GT}$ mice (Weber et al., 2002; Karlstetter et al., 2014), both genetic models for retinal degenerations, underlining the essential

role of IFNAR-signaling in retinal pathologies and microglial activation.
In conclusion, the results display an essential role of Ifnar-signaling, specifically in microglia cells during AMD-like retinal pathology.

## 4.4 The beneficial effect of IFN-$\beta$ therapy on disease symptoms

Since interferon beta is the first-line drug to treat relapsing remitting multiple sclerosis (RRMS) (Steinman et al., 2012) and inhibits the model disease EAE via different cellular and humoral mechanisms (Inoue and Shinohara, 2013), the aim of this approach was to analyze the immunomodulatory potential of IFN-$\beta$ in retinal pathologies. Using again the laser-coagulation model, our data clearly revealed decreased microgliosis, as there is a smaller amount of activated microglia cells in the lesion sites as well as CNV formation. These findings are in line with another IFN-$\beta$ therapy study, in which systemic IFN-$\beta$ administration was tested in a rabbit CNV model (Yasukawa et al., 2002). In this study, neovascularization was triggered by subretinal injection of gelatin microspheres containing basic fibroblast growth factor (bFGF). A following systemic therapy with diethylenetriaminepentaacetic acid (DTPA)-dextran conjugated IFNß has an inhibitory effect on CNV formation on early time points but did not affect CNV progression in later phases (Yasukawa et al., 2002). In contrast, these results show a remarkable therapeutic effect of IFN-$\beta$ especially in the late phase 14 days post laser damage. The crucial difference between both therapy studies could be the way CNV formation was triggered. The laser-coagulation model triggers CNV formation by inducing focal inflammatory sites into the retina by rupturing the Bruch's membrane, whereas the bFGF-induced model triggers angiogenesis by forming neovascular membrane scars. In accordance to this methodical distinction, IFN-$\beta$ treatment ameliorated laser-induced CNV in rabbits (Kimoto et al., 2002) and monkeys (Tobe et al., 1995). Of note, a patient suffering MS and punctate inner choroidopathy could significantly profit from systemic IFN-$\beta$ therapy and was subsequently free of CNV (Cirino et al., 2006).
Moreover, it has been published that IFN-$\beta$ treatment has a protective effect on experimental autoimmune uveoretinitis (EAU), a model disease for human intraocular inflammation, by suppressing Th1 and Th17 cells (Sun et al., 2011). Also primary cell culture experiments underline the protective effect of IFNß counteracting the neurotoxic activation state of microglial cells (Jin et al., 2007).
As the vascular endothelial growth factor (VEGF) is the main mediator of CVN

formation (Noel et al., 2007), anti-VEGF therapies are currently the therapy standard to treat the wet form of AMD (Rofagha et al., 2013; Rosenfeld et al., 2006). An ongoing challenge in these days is that there is currently no reliable therapy option for dry AMD (Jager et al., 2008). However, anti-VEGF therapy does not achieves the same anti-angiogenic effects in all patients and there are up to 30% non-responders (Amoaku et al., 2015; Otsuji et al., 2013). Hence, an alternative therapy option would be particularly interesting for anti-VEGF non-responders. Based on the results of this work, IFN-$\beta$ treatment is a conceivable new therapy option as it operates in an immunomodulatory mode of action.

To sum up, IFN-$\beta$ therapy significantly prevented microglial reactivity, and CNV formation. Hence, the protective mechanism of IFN-$\beta$ treatment might be an interesting new therapy option to especially treat AMD and other chronic inflammatory and degenerative diseases of the retina in an immunomodulatory manner.

## 4.5 Perspectives

In conclusion, findings of this study demonstrate for the first time the use of IFN-$\beta$ treatment as an alternative therapy option to ameliorate an AMD-like retinal pathology.

However, despite the depth of the current study which went as far as clearly underlining the beneficial effect of the IFNAR-signaling cascade on the disease course, the underlying molecular mechanisms still remain unclear. Thus, further experiments to identify possible mechanisms of action would be helpful in understanding how the IFNAR signaling pathway works to mediate the observed protective effects during experimentally induced wet AMD.

In addition, further independent *in vivo* models are necessary to verify the effect of IFN-$\beta$ therapy reported in this work. In line with this, the retinopathy of prematurity (ROP) model which also combines both, microgliosis and angiogenesis features, would be suitable for such verification (Smith et al., 1994).

Working with the tamoxifen-inducible Cx3cr1$^{\mathrm{CreER}}$ mice enables discrimination between microglia cells and other Cx3cr1-expressing monocytic cells due to their longevity. Despite of this difference, additional experiments differentiating more precisely between resident microglia, long-living macrophages and other Cx3cr1-expressing cells could help clarifying the actual contribution of retinal microglia to AMD-like retinal degeneration.

# Bibliography


Ajami, B., J. L. Bennett, C. Krieger, W. Tetzlaff, and F. M. Rossi
2007. Local self-renewal can sustain cns microglia maintenance and function throughout adult life. *Nat Neurosci*, 10(12):1538–43.

Amoaku, W. M., U. Chakravarthy, R. Gale, M. Gavin, F. Ghanchi, J. Gibson, S. Harding, R. L. Johnston, S. Kelly, A. Lotery, S. Mahmood, G. Menon, S. Sivaprasad, J. Talks, A. Tufail, and Y. Yang
2015. Defining response to anti-vegf therapies in neovascular amd. *Eye (Lond)*, 29(6):721–31.

Apte, R. S., J. Richter, J. Herndon, and T. A. Ferguson
2006. Macrophages inhibit neovascularization in a murine model of age-related macular degeneration. *PLoS Med*, 3(8):e310.

Aslanidis, A., M. Karlstetter, R. Scholz, S. Fauser, H. Neumann, C. Fried, M. Pietsch, and T. Langmann
2015. Activated microglia/macrophage whey acidic protein (amwap) inhibits nfkappab signaling and induces a neuroprotective phenotype in microglia. *J Neuroinflammation*, 12:77.

Autieri, M. V.
1996. cdna cloning of human allograft inflammatory factor-1: tissue distribution, cytokine induction, and mrna expression in injured rat carotid arteries. *Biochem Biophys Res Commun*, 228(1):29–37.

Banati, R. B., J. Gehrmann, P. Schubert, and G. W. Kreutzberg
1993. Cytotoxicity of microglia. *Glia*, 7(1):111–8.

Bekisz, J., H. Schmeisser, J. Hernandez, N. D. Goldman, and K. C. Zoon
2004. Human interferons alpha, beta and omega. *Growth Factors*, 22(4):243–51.

Blasi, E., R. Barluzzi, V. Bocchini, R. Mazzolla, and F. Bistoni
1990. Immortalization of murine microglial cells by a v-raf/v-myc carrying retrovirus. *J Neuroimmunol*, 27(2-3):229–37.

Bradford, M. M.
1976. A rapid and sensitive method for the quantitation of microgram quantities of protein utilizing the principle of protein-dye binding. *Anal Biochem*, 72:248–54.

Bringmann, A., T. Pannicke, J. Grosche, M. Francke, P. Wiedemann, S. N. Skatchkov, N. N. Osborne, and A. Reichenbach
2006. Muller cells in the healthy and diseased retina. *Prog Retin Eye Res*, 25(4):397–424.

Cardona, A. E., E. P. Pioro, M. E. Sasse, V. Kostenko, S. M. Cardona, I. M. Dijkstra, D. Huang, G. Kidd, S. Dombrowski, R. Dutta, J. C. Lee, D. N. Cook, S. Jung, S. A. Lira, D. R. Littman, and R. M. Ransohoff
2006. Control of microglial neurotoxicity by the fractalkine receptor. *Nat Neurosci*, 9(7):917–24.

Carter, D. A. and A. D. Dick
2004. Cd200 maintains microglial potential to migrate in adult human retinal explant model. *Curr Eye Res*, 28(6):427–36.

Chabot, S., G. Williams, and V. W. Yong
1997. Microglial production of tnf-alpha is induced by activated t lymphocytes. involvement of vla-4 and inhibition by interferonbeta-1b. *J Clin Invest*, 100(3):604–12.

Cirino, A. C., J. Mathura, J. R., and L. M. Jampol
2006. Resolution of activity (choroiditis and choroidal neovascularization) of chronic recurrent punctate inner choroidopathy after treatment with interferon b-1a. *Retina*, 26(9):1091–2.

Combadiere, C., C. Feumi, W. Raoul, N. Keller, M. Rodero, A. Pezard, S. Lavalette, M. Houssier, L. Jonet, E. Picard, P. Debre, M. Sirinyan, P. Deterre, T. Ferroukhi, S. Y. Cohen, D. Chauvaud, J. C. Jeanny, S. Chemtob, F. Behar-Cohen, and F. Sennlaub
2007. Cx3cr1-dependent subretinal microglia cell accumulation is associated with cardinal features of age-related macular degeneration. *J Clin Invest*, 117(10):2920–8.

Cooksley, W. G.
2004. The role of interferon therapy in hepatitis b. *MedGenMed*, 6(1):16.

de Jong, P. T.
2006. Age-related macular degeneration. *N Engl J Med*, 355(14):1474–85.

del Rio Hortega, P.
1932. Microglia. in: Cytology and cellular pathology of the nervous system, edited by penfield w. new york: Hoeber, 1932, p.482-1924-534. Pp. 481–534.

Detje, C. N., T. Meyer, H. Schmidt, D. Kreuz, J. K. Rose, I. Bechmann, M. Prinz, and U. Kalinke
2009. Local type i ifn receptor signaling protects against virus spread within the central nervous system. *J Immunol*, 182(4):2297–304.

Dick, A. D., A. L. Ford, J. V. Forrester, and J. D. Sedgwick
1995. Flow cytometric identification of a minority population of mhc class ii positive cells in the normal rat retina distinct from cd45lowcd11b/c+cd4low parenchymal microglia. *Br J Ophthalmol*, 79(9):834–40.

Dirscherl, K., M. Karlstetter, S. Ebert, D. Kraus, J. Hlawatsch, Y. Walczak, C. Moehle, R. Fuchshofer, and T. Langmann
2010. Luteolin triggers global changes in the microglial transcriptome leading to a unique anti-inflammatory and neuroprotective phenotype. *J Neuroinflammation*, 7:3.

Ebert, S., Y. Walczak, C. Reme, and T. Langmann
2012. Microglial activation and transcriptomic changes in the blue light-exposed mouse retina. *Adv Exp Med Biol*, 723:619–32.

Ebert, S., K. Weigelt, Y. Walczak, W. Drobnik, R. Mauerer, D. A. Hume, B. H. Weber, and T. Langmann
2009. Docosahexaenoic acid attenuates microglial activation and delays early retinal degeneration. *J Neurochem*, 110(6):1863–75.

Ejlerskov, P., J. G. Hultberg, J. Wang, R. Carlsson, M. Ambjorn, M. Kuss, Y. Liu, G. Porcu, K. Kolkova, C. Friis Rundsten, K. Ruscher, B. Pakkenberg, T. Goldmann, D. Loreth, M. Prinz, D. C. Rubinsztein, and S. Issazadeh-Navikas
2015. Lack of neuronal ifn-beta-ifnar causes lewy body- and parkinson's disease-like dementia. *Cell*, 163(2):324–39.

Engelhardt, B. and S. Liebner
2014. Novel insights into the development and maintenance of the blood-brain barrier. *Cell Tissue Res*, 355(3):687–99.

Espinosa-Heidmann, D. G., I. J. Suner, E. P. Hernandez, D. Monroy, K. G. Csaky, and S. W. Cousins
2003. Macrophage depletion diminishes lesion size and severity in experimental choroidal neovascularization. *Invest Ophthalmol Vis Sci*, 44(8):3586–92.

Eter, N., D. R. Engel, L. Meyer, H. M. Helb, F. Roth, J. Maurer, F. G. Holz, and C. Kurts
2008. In vivo visualization of dendritic cells, macrophages, and microglial cells responding to laser-induced damage in the fundus of the eye. *Invest Ophthalmol Vis Sci*, 49(8):3649–58.

Foster, G. R., C. Germain, M. Jones, R. I. Lechler, and G. Lombardi
2000. Human t cells elicit ifn-alpha secretion from dendritic cells following cell to cell interactions. *Eur J Immunol*, 30(11):3228–35.

Friedman, R. M.
2008. Clinical uses of interferons. *Br J Clin Pharmacol*, 65(2):158–62.

Gao, H. M., H. Zhou, F. Zhang, B. C. Wilson, W. Kam, and J. S. Hong
2011. Hmgb1 acts on microglia mac1 to mediate chronic neuroinflammation that drives progressive neurodegeneration. *J Neurosci*, 31(3):1081–92.

Gehrmann, J., Y. Matsumoto, and G. W. Kreutzberg
1995. Microglia: intrinsic immuneffector cell of the brain. *Brain Res Brain Res Rev*, 20(3):269–87.

Ginhoux, F., M. Greter, M. Leboeuf, S. Nandi, P. See, S. Gokhan, M. F. Mehler, S. J. Conway, L. G. Ng, E. R. Stanley, I. M. Samokhvalov, and M. Merad
2010. Fate mapping analysis reveals that adult microglia derive from primitive macrophages. *Science*, 330(6005):841–5.

Goldmann, T., P. Wieghofer, P. F. Muller, Y. Wolf, D. Varol, S. Yona, S. M. Brendecke, K. Kierdorf, O. Staszewski, M. Datta, T. Luedde, M. Heikenwalder, S. Jung, and M. Prinz
2013. A new type of microglia gene targeting shows tak1 to be pivotal in cns autoimmune inflammation. *Nat Neurosci*, 16(11):1618–26.

Goldmann, T., N. Zeller, J. Raasch, K. Kierdorf, K. Frenzel, L. Ketscher, A. Basters, O. Staszewski, S. M. Brendecke, A. Spiess, T. L. Tay, C. Kreutz, J. Timmer, G. M. Mancini, T. Blank, G. Fritz, K. Biber, R. Lang, D. Malo, D. Merkler, M. Heikenwalder, K. P. Knobeloch, and M. Prinz
2015. Usp18 lack in microglia causes destructive interferonopathy of the mouse brain. *Embo j*, 34(12):1612–29.

Gong, Y., J. Li, Y. Sun, Z. Fu, C. H. Liu, L. Evans, K. Tian, N. Saba, T. Fredrick, P. Morss, J. Chen, and L. E. Smith
2015. Optimization of an image-guided laser-induced choroidal neovascularization model in mice. *PLoS One*, 10(7):e0132643.

Gresser, I. and C. Bourali
1970. Antitumor effects of interferon preparations in mice. *J Natl Cancer Inst*, 45(2):365–76.

Gupta, N., K. E. Brown, and A. H. Milam
2003. Activated microglia in human retinitis pigmentosa, late-onset retinal degeneration, and age-related macular degeneration. *Exp Eye Res*, 76(4):463–71.

Hardy, M. P., C. M. Owczarek, L. S. Jermiin, M. Ejdeback, and P. J. Hertzog
2004. Characterization of the type i interferon locus and identification of novel genes. *Genomics*, 84(2):331–45.

Holland, P. M., R. D. Abramson, R. Watson, and D. H. Gelfand
1991. Detection of specific polymerase chain reaction product by utilizing the 5'—-3' exonuclease activity of thermus aquaticus dna polymerase. *Proc Natl Acad Sci U S A*, 88(16):7276–80.

Inoue, M. and M. L. Shinohara
2013. The role of interferon-beta in the treatment of multiple sclerosis and experimental autoimmune encephalomyelitis - in the perspective of inflammasomes. *Immunology*, 139(1):11–8.

Isaacs, A. and J. Lindenmann
1987. Virus interference. i. the interferon. by a. isaacs and j. lindenmann, 1957. *J Interferon Res*, 7(5):429–38.

Ito, D., Y. Imai, K. Ohsawa, K. Nakajima, Y. Fukuuchi, and S. Kohsaka
1998. Microglia-specific localisation of a novel calcium binding protein, iba1. *Brain Res Mol Brain Res*, 57(1):1–9.

Jacobs, L., J. O'Malley, A. Freeman, J. Murawski, and R. Ekes
1982. Intrathecal interferon in multiple sclerosis. *Arch Neurol*, 39(10):609–15.

Jager, R. D., W. F. Mieler, and J. W. Miller
2008. Age-related macular degeneration. *N Engl J Med*, 358(24):2606–17.

Jin, S., J. Kawanokuchi, T. Mizuno, J. Wang, Y. Sonobe, H. Takeuchi, and A. Suzumura
2007. Interferon-beta is neuroprotective against the toxicity induced by activated microglia. *Brain Res*, 1179:140–6.

Karlstetter, M., S. Ebert, and T. Langmann
2010. Microglia in the healthy and degenerating retina: insights from novel mouse models. *Immunobiology*, 215(9-10):685–91. 1878-3279 Karlstetter, Marcus Ebert, Stefanie Langmann, Thomas Journal Article Research Support, Non-U.S. Gov't Review Netherlands Immunobiology. 2010 Sep-Oct;215(9-10):685-91. doi: 10.1016/j.imbio.2010.05.010. Epub 2010 Jun 4.

Karlstetter, M. and T. Langmann
2014. Microglia in the aging retina. *Adv Exp Med Biol*, 801:207–12.

Karlstetter, M., E. Lippe, Y. Walczak, C. Moehle, A. Aslanidis, M. Mirza, and T. Langmann
2011. Curcumin is a potent modulator of microglial gene expression and migration. *J Neuroinflammation*, 8:125.

Karlstetter, M., R. Scholz, M. Rutar, W. T. Wong, J. M. Provis, and T. Langmann
2015. Retinal microglia: just bystander or target for therapy? *Prog Retin Eye Res*, 45:30–57.

Karlstetter, M., N. Sorusch, A. Caramoy, K. Dannhausen, A. Aslanidis, S. Fauser, M. R. Boesl, K. Nagel-Wolfrum, E. R. Tamm, H. Jagle, H. Stoehr, U. Wolfrum, and T. Langmann
2014. Disruption of the retinitis pigmentosa 28 gene fam161a in mice affects photoreceptor ciliary structure and leads to progressive retinal degeneration. *Hum Mol Genet*, 23(19):5197–210.

Kettenmann, H., U. K. Hanisch, M. Noda, and A. Verkhratsky
2011. Physiology of microglia. *Physiol Rev*, 91(2):461–553.

Khorooshi, R., M. T. Morch, T. H. Holm, C. T. Berg, R. T. Dieu, D. Draeby, S. Issazadeh-Navikas, S. Weiss, S. Lienenklaus, and T. Owens
2015. Induction of endogenous type i interferon within the central nervous system plays a protective role in experimental autoimmune encephalomyelitis. *Acta Neuropathol*, 130(1):107–18.

Kierdorf, K., D. Erny, T. Goldmann, V. Sander, C. Schulz, E. G. Perdiguero, P. Wieghofer, A. Heinrich, P. Riemke, C. Holscher, D. N. Muller, B. Luckow, T. Brocker, K. Debowski, G. Fritz, G. Opdenakker, A. Diefenbach, K. Biber, M. Heikenwalder, F. Geissmann, F. Rosenbauer, and M. Prinz
2013. Microglia emerge from erythromyeloid precursors via pu.1- and irf8-dependent pathways. *Nat Neurosci*, 16(3):273–80.

Kieseier, B. C.
2011. The mechanism of action of interferon-beta in relapsing multiple sclerosis. *CNS Drugs*, 25(6):491–502.

Killingsworth, M. C., J. P. Sarks, and S. H. Sarks
1990. Macrophages related to bruch's membrane in age-related macular degeneration. *Eye (Lond)*, 4 ( Pt 4):613–21.

Kimoto, T., K. Takahashi, T. Tobe, K. Fujimoto, M. Uyama, and S. Sone
2002. Effects of local administration of interferon-beta on proliferation of retinal pigment epithelium in rabbit after laser photocoagulation. *Jpn J Ophthalmol*, 46(2):160–9.

Kleppe, K., E. Ohtsuka, R. Kleppe, I. Molineux, and H. G. Khorana
1971. Studies on polynucleotides. xcvi. repair replications of short synthetic dna's as catalyzed by dna polymerases. *J Mol Biol*, 56(2):341–61.

Kocur, M., R. Schneider, A. K. Pulm, J. Bauer, S. Kropp, M. Gliem, J. Ingwersen, N. Goebels, J. Alferink, T. Prozorovski, O. Aktas, and S. Scheu
2015. Ifnbeta secreted by microglia mediates clearance of myelin debris in cns autoimmunity. *Acta Neuropathol Commun*, 3:20.

Kreutzberg, G. W.
1996. Microglia: a sensor for pathological events in the cns. *Trends in Neurosciences*, 19(8):312–318.

Krown, S. E., M. W. Burk, J. M. Kirkwood, D. Kerr, D. L. Morton, and H. F. Oettgen
1984. Human leukocyte (alpha) interferon in metastatic malignant melanoma: the american cancer society phase ii trial. *Cancer Treat Rep*, 68(5):723–6.

Lambert, V., J. Lecomte, S. Hansen, S. Blacher, M. L. Gonzalez, I. Struman, N. E. Sounni, E. Rozet, P. de Tullio, J. M. Foidart, J. M. Rakic, and A. Noel
2013. Laser-induced choroidal neovascularization model to study age-related macular degeneration in mice. *Nat Protoc*, 8(11):2197–211.

Langmann, T.
2007. Microglia activation in retinal degeneration. *J Leukoc Biol*, 81(6):1345–51.

Liebner, S., C. J. Czupalla, and H. Wolburg
2011. Current concepts of blood-brain barrier development. *Int J Dev Biol*, 55(4-5):467–76.

Liu, J., D. A. Copland, S. Horie, W. K. Wu, M. Chen, Y. Xu, B. Paul Morgan, M. Mack, H. Xu, L. B. Nicholson, and A. D. Dick
2013. Myeloid cells expressing vegf and arginase-1 following uptake of damaged retinal pigment epithelium suggests potential mechanism that drives the onset of choroidal angiogenesis in mice. *PLoS One*, 8(8):e72935.

Liu, Y. J.
2005. Ipc: professional type 1 interferon-producing cells and plasmacytoid dendritic cell precursors. *Annu Rev Immunol*, 23:275–306.

Louie, A. C., J. G. Gallagher, K. Sikora, R. Levy, S. A. Rosenberg, and T. C. Merigan
1981. Follow-up observations on the effect of human leukocyte interferon in non-hodgkin's lymphoma. *Blood*, 58(4):712–8.

Lueckoff, A., A. Caramoy, R. Scholz, M. Prinz, U. Kalinke, and T. Langmann
2016. Interferon-beta signaling in retinal mononuclear phagocytes attenuates pathological neovascularization. *EMBO Mol Med*.

Luhmann, U. F., C. A. Lange, S. Robbie, P. M. Munro, J. A. Cowing, H. E. Armer, V. Luong, L. S. Carvalho, R. E. MacLaren, F. W. Fitzke, J. W. Bainbridge, and R. R. Ali
2012. Differential modulation of retinal degeneration by ccl2 and cx3cr1 chemokine signalling. *PLoS One*, 7(4):e35551.

McMenamin, P. G.
1999. Dendritic cells and macrophages in the uveal tract of the normal mouse eye. *Br J Ophthalmol*, 83(5):598–604.

Muller, U., U. Steinhoff, L. F. Reis, S. Hemmi, J. Pavlovic, R. M. Zinkernagel, and M. Aguet
1994. Functional role of type i and type ii interferons in antiviral defense. *Science*, 264(5167):1918–21.

Newman, A. M., N. B. Gallo, L. S. Hancox, N. J. Miller, C. M. Radeke, M. A. Maloney, J. B. Cooper, G. S. Hageman, D. H. Anderson, L. V. Johnson, and M. J. Radeke
2012. Systems-level analysis of age-related macular degeneration reveals global biomarkers and phenotype-specific functional networks. *Genome Med*, 4(2):16.

Nicholls, J., A. Martin, B. Wallache, and P. Fuchs
2001. From neuron to brain. *Sinauer*, 4th edition.

Nikfar, S., R. Rahimi, and M. Abdollahi
2010. A meta-analysis of the efficacy and tolerability of interferon-beta in multiple sclerosis, overall and by drug and disease type. *Clin Ther*, 32(11):1871–88.

Nimmerjahn, A., F. Kirchhoff, and F. Helmchen
2005. Resting microglial cells are highly dynamic surveillants of brain parenchyma in vivo. *Science*, 308(5726):1314–8.

Noel, A., M. Jost, V. Lambert, J. Lecomte, and J. M. Rakic
2007. Anti-angiogenic therapy of exudative age-related macular degeneration: current progress and emerging concepts. *Trends Mol Med*, 13(8):345–52.

Oritani, K., K. L. Medina, Y. Tomiyama, J. Ishikawa, Y. Okajima, M. Ogawa, T. Yokota, K. Aoyama, I. Takahashi, P. W. Kincade, and Y. Matsuzawa
2000. Limitin: An interferon-like cytokine that preferentially influences b-lymphocyte precursors. *Nat Med*, 6(6):659–66.

Otsuji, T., Y. Nagai, K. Sho, A. Tsumura, N. Koike, M. Tsuda, T. Nishimura, and K. Takahashi
2013. Initial non-responders to ranibizumab in the treatment of age-related macular degeneration (amd). *Clin Ophthalmol*, 7:1487–90.

Parkin, J. and B. Cohen
2001. An overview of the immune system. *Lancet*, 357(9270):1777–89.

Paty, D. W. and D. K. Li
2001. Interferon beta-lb is effective in relapsing-remitting multiple sclerosis. ii. mri analysis results of a multicenter, randomized, double-blind, placebo-controlled trial. 1993 [classical article]. *Neurology*, 57(12 Suppl 5):S10–5.

Penfold, P. L., M. C. Killingsworth, and S. H. Sarks
1985. Senile macular degeneration: the involvement of immunocompetent cells. *Graefes Arch Clin Exp Ophthalmol*, 223(2):69–76.

Pennesi, M. E., M. Neuringer, and R. J. Courtney
2012. Animal models of age related macular degeneration. *Mol Aspects Med*, 33(4):487–509.

Pestka, S., C. D. Krause, and M. R. Walter
2004. Interferons, interferon-like cytokines, and their receptors. *Immunol Rev*, 202:8–32.

Pestka, S., J. A. Langer, K. C. Zoon, and C. E. Samuel
1987. Interferons and their actions. *Annu Rev Biochem*, 56:727–77.

Portera-Cailliau, C., C. H. Sung, J. Nathans, and R. Adler
1994. Apoptotic photoreceptor cell death in mouse models of retinitis pigmentosa. *Proc Natl Acad Sci U S A*, 91(3):974–8.

Prinz, M., H. Schmidt, A. Mildner, K. P. Knobeloch, U. K. Hanisch, J. Raasch, D. Merkler, C. Detje, I. Gutcher, J. Mages, R. Lang, R. Martin, R. Gold, B. Becher, W. Bruck, and U. Kalinke
2008. Distinct and nonredundant in vivo functions of ifnar on myeloid cells limit autoimmunity in the central nervous system. *Immunity*, 28(5):675–86.

Quesada, J. R., D. A. Swanson, A. Trindade, and J. U. Gutterman
1983. Renal cell carcinoma: antitumor effects of leukocyte interferon. *Cancer Res*, 43(2):940–7.

Ransohoff, R. M. and A. E. Cardona
2010. The myeloid cells of the central nervous system parenchyma. *Nature*, 468(7321):253–62.

Reiner, A., S. A. Heldt, C. S. Presley, N. H. Guley, A. J. Elberger, Y. Deng, L. D'Surney, J. T. Rogers, J. Ferrell, W. Bu, N. Del Mar, M. G. Honig, S. N. Gurley, and n. Moore, B. M.
2015. Motor, visual and emotional deficits in mice after closed-head mild traumatic brain injury are alleviated by the novel cb2 inverse agonist smm-189. *Int J Mol Sci*, 16(1):758–87.

Rofagha, S., R. B. Bhisitkul, D. S. Boyer, S. R. Sadda, K. Zhang, and S.-U. S. Group
2013. Seven-year outcomes in ranibizumab-treated patients in anchor, marina, and horizon: a multicenter cohort study (seven-up). *Ophthalmology*, 120(11):2292–9.

Rosenfeld, P. J., D. M. Brown, J. S. Heier, D. S. Boyer, P. K. Kaiser, C. Y. Chung, and R. Y. Kim
2006. Ranibizumab for neovascular age-related macular degeneration. *N Engl J Med*, 355(14):1419–31.

Ryan, S. J.
1979. The development of an experimental model of subretinal neovascularization in disciform macular degeneration. *Trans Am Ophthalmol Soc*, 77:707–45.

Sabatel, C., L. Malvaux, N. Bovy, C. Deroanne, V. Lambert, M. L. Gonzalez, A. Colige, J. M. Rakic, A. Noel, J. A. Martial, and I. Struman
2011. Microrna-21 exhibits antiangiogenic function by targeting rhob expression in endothelial cells. *PLoS One*, 6(2):e16979.

Sadler, A. J. and B. R. Williams
2008. Interferon-inducible antiviral effectors. *Nat Rev Immunol*, 8(7):559–68.

Saishin, Y., Y. Saishin, K. Takahashi, R. Lima e Silva, D. Hylton, J. S. Rudge, S. J. Wiegand, and P. A. Campochiaro
2003. Vegf-trap(r1r2) suppresses choroidal neovascularization and vegf-induced breakdown of the blood-retinal barrier. *J Cell Physiol*, 195(2):241–8.

Sakurai, E., A. Anand, B. K. Ambati, N. van Rooijen, and J. Ambati
2003. Macrophage depletion inhibits experimental choroidal neovascularization. *Invest Ophthalmol Vis Sci*, 44(8):3578–85.

Scholz, R., A. Caramoy, M. B. Bhuckory, K. Rashid, M. Chen, H. Xu, C. Grimm, and T. Langmann
2015a. Targeting translocator protein (18 kda) (tspo) dampens pro-inflammatory microglia reactivity in the retina and protects from degeneration. *J Neuroinflammation*, 12(1):201.

Scholz, R., M. Sobotka, A. Caramoy, T. Stempfl, C. Moehle, and T. Langmann
2015b. Minocycline counter-regulates pro-inflammatory microglia responses in the retina and protects from degeneration. *J Neuroinflammation*, 12:209.

Schuetz, E. and S. Thanos
2004. Microglia-targeted pharmacotherapy in retinal neurodegenerative diseases. *Curr Drug Targets*, 5(7):619–27.

Schulz, C., E. Gomez Perdiguero, L. Chorro, H. Szabo-Rogers, N. Cagnard, K. Kierdorf, M. Prinz, B. Wu, S. E. Jacobsen, J. W. Pollard, J. Frampton, K. J. Liu, and F. Geissmann
2012. A lineage of myeloid cells independent of myb and hematopoietic stem cells. *Science*, 336(6077):86–90.

Shen, W. Y., M. J. Yu, C. J. Barry, I. J. Constable, and P. E. Rakoczy
1998. Expression of cell adhesion molecules and vascular endothelial growth factor in experimental choroidal neovascularisation in the rat. *Br J Ophthalmol*, 82(9):1063–71.

Shepherd, J., N. Waugh, and P. Hewitson
2000. Combination therapy (interferon alfa and ribavirin) in the treatment of chronic hepatitis c: a rapid and systematic review. *Health Technol Assess*, 4(33):1–67.

Slakter, J. S.
2006. Anecortave acetate for treating or preventing choroidal neovascularization. *Ophthalmol Clin North Am*, 19(3):373–80.

Smith, L. E., E. Wesolowski, A. McLellan, S. K. Kostyk, R. D'Amato, R. Sullivan, and P. A. D'Amore
1994. Oxygen-induced retinopathy in the mouse. *Invest Ophthalmol Vis Sci*, 35(1):101–11.

Soriano, P.
1999. Generalized lacz expression with the rosa26 cre reporter strain. *Nat Genet*, 21(1):70–1.

Stark, G. R., I. M. Kerr, B. R. Williams, R. H. Silverman, and R. D. Schreiber
1998. How cells respond to interferons. *Annu Rev Biochem*, 67:227–64.

Steinman, L., J. T. Merrill, I. B. McInnes, and M. Peakman
2012. Optimization of current and future therapy for autoimmune diseases. *Nat Med*, 18(1):59–65.

Strauss, O.
2005. The retinal pigment epithelium in visual function. *Physiol Rev*, 85(3):845–81.

Streit, W. J.
2002. Microglia as neuroprotective, immunocompetent cells of the cns. *Glia*, 40(2):133–9.

study, G. b. o. d.
2015. Global, regional, and national incidence, prevalence, and years lived with disability for 301 acute and chronic diseases and injuries in 188 countries, 1990-2013: a systematic analysis for the global burden of disease study 2013. *Lancet*, 386(9995):743–800.

Sun, M., Y. Yang, P. Yang, B. Lei, L. Du, and A. Kijlstra
2011. Regulatory effects of ifn-beta on the development of experimental autoimmune uveoretinitis in b10riii mice. *PLoS One*, 6(5):e19870.

Sundaram, V., A. T. Moore, R. R. Ali, and J. W. Bainbridge
2012. Retinal dystrophies and gene therapy. *Eur J Pediatr*, 171(5):757–65.

Sung, C. H. and J. Z. Chuang
2010. The cell biology of vision. *J Cell Biol*, 190(6):953–63.

Taniguchi, T., Y. Fujii-Kuriyama, and M. Muramatsu
1980. Molecular cloning of human interferon cdna. *Proc Natl Acad Sci U S A*, 77(7):4003–6.

Teige, I., A. Treschow, A. Teige, R. Mattsson, V. Navikas, T. Leanderson, R. Holmdahl, and S. Issazadeh-Navikas
2003. Ifn-beta gene deletion leads to augmented and chronic demyelinating experimental autoimmune encephalomyelitis. *J Immunol*, 170(9):4776–84.

Tilg, H. and A. M. Diehl
2000. Cytokines in alcoholic and nonalcoholic steatohepatitis. *N Engl J Med*, 343(20):1467–76.

Tobe, T., S. Ortega, J. D. Luna, H. Ozaki, N. Okamoto, N. L. Derevjanik, S. A. Vinores, C. Basilico, and P. A. Campochiaro
1998. Targeted disruption of the fgf2 gene does not prevent choroidal neovascularization in a murine model. *Am J Pathol*, 153(5):1641–6.

Tobe, T., K. Takahashi, H. Ohkuma, and M. Uyama
1995. [the effect of interferon-beta on experimental choroidal neovascularization]. *Nippon Ganka Gakkai Zasshi*, 99(5):571–81.

Tracey, K. J. and A. Cerami
1993. Tumor necrosis factor, other cytokines and disease. *Annu Rev Cell Biol*, 9:317–43.

Uze, G., G. Schreiber, J. Piehler, and S. Pellegrini
2007. The receptor of the type i interferon family. *Curr Top Microbiol Immunol*, 316:71–95.

van Rossum, D. and U. K. Hanisch
2004. Microglia. *Metab Brain Dis*, 19(3-4):393–411.

Weber, B. H., H. Schrewe, L. L. Molday, A. Gehrig, K. L. White, M. W. Seeliger, G. B. Jaissle, C. Friedburg, E. Tamm, and R. S. Molday
2002. Inactivation of the murine x-linked juvenile retinoschisis gene, rs1h, suggests a role of retinoschisin in retinal cell layer organization and synaptic structure. *Proc Natl Acad Sci U S A*, 99(9):6222–7.

Wieghofer, P., K. P. Knobeloch, and M. Prinz
2015. Genetic targeting of microglia. *Glia*, 63(1):1–22.

Xu, H., M. Chen, E. J. Mayer, J. V. Forrester, and A. D. Dick
2007. Turnover of resident retinal microglia in the normal adult mouse. *Glia*, 55(11):1189–98.

Yasukawa, T., H. Kimura, Y. Tabata, H. Kamizuru, H. Miyamoto, Y. Honda, and Y. Ogura
2002. Targeting of interferon to choroidal neovascularization by use of dextran and metal coordination. *Invest Ophthalmol Vis Sci*, 43(3):842–8.

Yona, S., K. W. Kim, Y. Wolf, A. Mildner, D. Varol, M. Breker, D. Strauss-Ayali, S. Viukov, M. Guilliams, A. Misharin, D. A. Hume, H. Perlman, B. Malissen, E. Zelzer, and S. Jung
2013. Fate mapping reveals origins and dynamics of monocytes and tissue macrophages under homeostasis. *Immunity*, 38(1):79–91.

Yong, V. W., S. Chabot, O. Stuve, and G. Williams
1998. Interferon beta in the treatment of multiple sclerosis: mechanisms of action. *Neurology*, 51(3):682–9.

Zhao, L., M. K. Zabel, X. Wang, W. Ma, P. Shah, R. N. Fariss, H. Qian, C. N. Parkhurst, W. B. Gan, and W. T. Wong
2015. Microglial phagocytosis of living photoreceptors contributes to inherited retinal degeneration. *EMBO Mol Med*, 7(9):1179–97.

# Abbreviations

| | |
|---|---|
| **Aif1** | Allograft inflammatory factor 1 |
| $\alpha_M\beta_2$ | Integrin alpha-M beta-2 |
| AMD | Age-related macular degeneration |
| Avg | Average |
| **BBB** | Blood brain barrier |
| BRB | Blood retina barrier |
| bp | Base pairs |
| BSA | Bovine serum albumin |
| bFGF | Basic fibroblast growth factor |
| **CHO** | Chinese hamster ovary cells |
| cDNA | Complementary DNA |
| CD11b | Cluster of differentiation molecule 11b |
| CNS | Central nervous system |
| CNV | Choroidal neovascularization |
| Cre | Causes recombination / Cyclization recombinase |
| CX3CR1 | C-X3-C motif chemokine receptor 1, also called fraktalkine |
| **$dH_2O$** | Distilled water |
| DAMP | Damage/danger-associated molecular pattern |
| DAPI | 4',6-Diamidino-2-phenylindol |
| DMEM | Dulbecco's modified eagle's medium |
| DNA | Deoxyribonucleic acid |
| dNTP's | 2'-desoyribonucleotides triphosphate |
| DTPA | Diethylenetriaminepentaacetic acid |
| **EAE** | Experimental autoimmune encephalomyelitis |
| EAU | Experimental autoimmune uveoretinitis |
| **F** | Forward |
| FFA | Fundus fluorescein angiography |
| Fig | Figure |
| FCS | Fetal calf serum |
| **GAPDH** | Glyceraldehyde 3-phosphate dehydrogenase |
| GT | Gene trap |
| **h** | Hours |
| H&E stain | Hematoxylin and eosin stain |

| | |
|---|---|
| HRP | Horseradisch peroxidase |
| **IFN** | Interferon |
| IFNAR | Interferon-$\alpha/\beta$ receptor |
| IFN-$\beta$ | Interferon-$\beta$ |
| Iba1 | Ionized calcium-binding adapter molecule 1 |
| i.p. | Intraperitoneal injection |
| IRF | Interferon-regulatory factor |
| ISG | Interferon-stimulated gene |
| ISG15 | Interferon-stimulated gene, 15 kDa |
| ISRE | Interferon-stimulated response element |
| i.v. | Introvenous injection |
| **Jak** | Janus kinase |
| JAK1 | Janus kinase 1 |
| **kDa** | Kilodalton |
| **LPS** | Lipopolysaccharide |
| **MHC** | Major histocompatibility complex |
| min | Minute |
| $\mu$g | Microgram |
| mg | Milligram |
| ml | Millilitre |
| MX1 | Myxovirus resistance 1 |
| MX2 | Myxovirus resistance 2 |
| **NaCl** | Sodium chloride |
| Na-DCA | Sodium deoxycholate |
| NaOH | Sodium hydroxide |
| nm | Nanometre |
| NO | Nitric oxide |
| NTC | Non Template Control |
| **OD** | Optical density |
| ONH | Optical nerve head |
| **PBS** | Phosphate buffered saline |
| PBS-T | Phosphate buffered saline-Tween20 |
| PCR | Polymerase chain reaction |
| PFA | Paraformaldehyde |
| **qRT-PCR** | Quantitative real-time polymerase chain reaction |

| | |
|---|---|
| **R** | Reverse |
| R26 | Rosa26 locus |
| RPE | Retinal pigment epithelium |
| RIPA | Radioimmunoprecipitation assay buffer |
| RNA | Ribonucleic acid |
| ROI | Region of interest |
| ROS | Reactive oxygen species |
| rpm | Revolutions per minute |
| RR-MS | Relapsing-remitting multiple sclerosis |
| RP | Retinitis Pigmentosa |
| RT | Room temperature |
| **sec** | Second |
| SD | Standard deviation |
| SDS | Sodium dodecyl sulfate |
| SDS-PAGE | Sodium dodecyl sulfate - polyacrylamide gel electrophoresis |
| SD-OCT | Spectral domain - optical coherence tomography |
| STAT | Signal transducer and activator of transcription |
| **Tab** | Table |
| TBS | Tris bufferes saline |
| Temed | Tetramethylethylendiamine |
| Tg | Transgen |
| TRITC | Tetramethylrhodamine |
| Tween20 | Polyoxyethylen-(20)-sorbitanmonolaurat |
| Tyk2 | Tyrosine kinase 2 |
| **U** | Unit |
| **VEGF** | Vascular endothelial growth factor |
| **WT** | Wild type |

# List of Figures

# List of Tables

# 5 Attachments

# Danksagung

This page only appears on the printed version of the thesis.

# Erklärung

Ich versichere, dass ich die von mir vorgelegte Dissertation selbständig angefertigt, die benutzten Quellen und Hilfsmittel vollständig angegeben und die Stellen der Arbeit - einschließlich Tabellen, Karten und Abbildungen -, die anderen Werken im Wortlaut oder dem Sinn nach entnommen sind, in jedem Einzelfall als Entlehnung kenntlich gemacht habe; dass diese Dissertation noch keiner anderen Fakultät oder Universität zur Prüfung vorgelegen hat; dass sie - abgesehen von unten angegebenen Teilpublikationen - noch nicht veröffentlicht worden ist sowie, dass ich eine solche Veröffentlichung vor Abschluss des Promotionsverfahrens nicht vornehmen werde. Die Bestimmungen der Promotionsordnung sind mir bekannt. Die von mir vorgelegte Dissertation ist von Prof. Dr. Elena Rugarli und Prof. Dr. Thomas Langmann betreut worden.

Köln, den 23.05.2016

Teilpublikation:

**Anika Lückoff**, Albert Caramoy, Rebecca Scholz, Marco Prinz, Ulrich Kalinke & Thomas Langmann (2016),
Interferon-beta signaling in retinal mononuclear phagocytes attenuates pathological neovascularization. EMBO Mol Med. doi: 10.15252/emmm.201505994

# Lebenslauf

This page only appears on the printed version of the thesis.